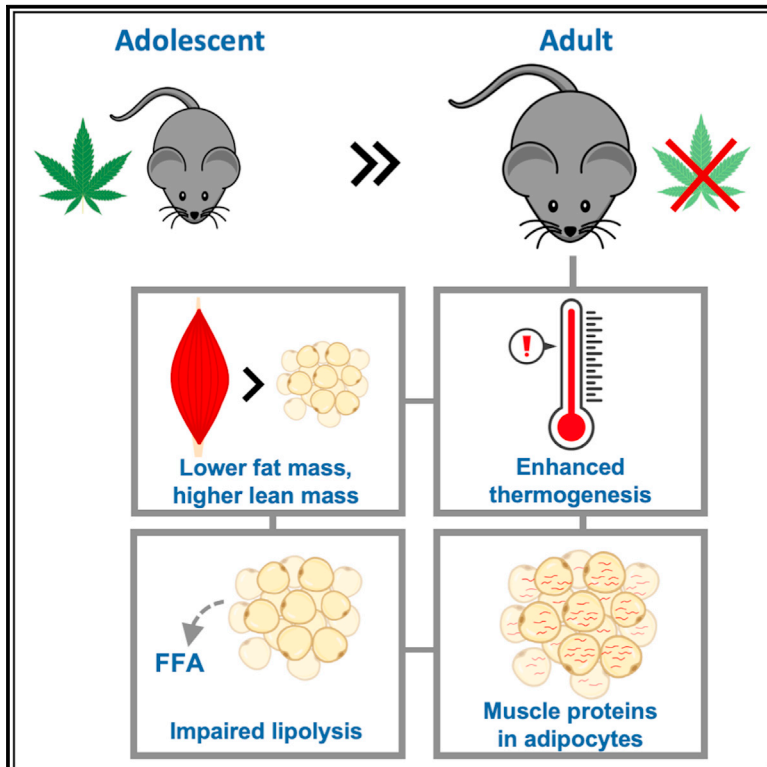


Cell Metabolism

Adolescent exposure to low-dose THC disrupts energy balance and adipose organ homeostasis in adulthood

Graphical abstract



Authors

Lin Lin, Kwang-Mook Jung, Hye-Lim Lee, ..., Cholsoon Jang, Saverio Cinti, Daniele Piomelli

Correspondence

piomelli@hs.uci.edu

In brief

Lin et al. report that treating adolescent mice with low-dose THC produces an adult metabolic phenotype in which apparently healthy features, such as leanness and an improved lipid panel, are accompanied by profound molecular and functional abnormalities, including the presence in fat of proteins that are normally found in muscle.

Highlights

- Exposing adolescent mice to low-dose THC alters their adult energy metabolism
- CB₁ receptor activation in differentiated adipocytes mediates this effect
- THC-treated mice are leaner than controls
- Molecular and functional adipose abnormalities identify this state as pseudo-lean

Article

Adolescent exposure to low-dose THC disrupts energy balance and adipose organ homeostasis in adulthood

Lin Lin,¹ Kwang-Mook Jung,^{1,7} Hye-Lim Lee,^{1,7} Johnny Le,² Georgia Colleluori,³ Courtney Wood,⁴ Francesca Palese,¹ Erica Squire,¹ Jade Ramirez,¹ Shiqi Su,¹ Alexa Torrens,¹ Yannick Fotio,¹ Lingyi Tang,⁵ Clinton Yu,⁵ Qin Yang,⁵ Lan Huang,⁵ Nicholas DiPatrizio,⁴ Cholsoon Jang,² Saverio Cinti,³ and Daniele Piomelli^{1,2,6,8,*}

¹Department of Anatomy and Neurobiology, University of California, Irvine, Irvine, CA 92697, USA

²Department of Biological Chemistry, University of California, Irvine, Irvine, CA 92697, USA

³Department of Clinical and Experimental Medicine, Center of Obesity, Marche Polytechnic University, Ancona 600126, Italy

⁴Department of Biomedical Sciences, University of California, Riverside, Riverside, CA 92697, USA

⁵Department of Physiology and Biophysics, University of California, Irvine, Irvine, CA 92697, USA

⁶Department of Pharmaceutical Sciences, University of California, Irvine, Irvine, CA 92697, USA

⁷These authors contributed equally

⁸Lead contact

*Correspondence: piomelli@hs.uci.edu

<https://doi.org/10.1016/j.cmet.2023.05.002>

SUMMARY

One of cannabis' most iconic effects is the stimulation of hedonic high-calorie eating—the “munchies”—yet habitual cannabis users are, on average, leaner than non-users. We asked whether this phenotype might result from lasting changes in energy balance established during adolescence, when use of the drug often begins. We found that daily low-dose administration of cannabis' intoxicating constituent, Δ^9 -tetrahydrocannabinol (THC), to adolescent male mice causes an adult metabolic phenotype characterized by reduced fat mass, increased lean mass and utilization of fat as fuel, partial resistance to diet-induced obesity and dyslipidemia, enhanced thermogenesis, and impaired cold- and β -adrenergic receptor-stimulated lipolysis. Further analyses revealed that this phenotype is associated with molecular anomalies in the adipose organ, including ectopic overexpression of muscle-associated proteins and heightened anabolic processing. Thus, adolescent exposure to THC may promote an enduring “pseudo-lean” state that superficially resembles healthy leanness but might in fact be rooted in adipose organ dysfunction.

INTRODUCTION

The endocannabinoid system (ECS) is found in most, if not all, mammalian organs and is involved in a diversity of physiological processes.^{1,2} It comprises two G protein-coupled receptors (CB₁ and CB₂), two lipid-derived ligands (anandamide and 2-arachidonoyl-*sn*-glycerol [2-AG]), and various enzymes and transporter proteins responsible for the formation, transfer, and degradation of such ligands.^{1,2} All constituents of the ECS are represented in white (WAT) and brown adipose tissues (BAT)—the parenchymal components of the adipose organ³—where endocannabinoid substances may act as “thrifty” autocrine/paracrine messengers^{4,5} to enhance lipogenesis and attenuate non-shivering thermogenesis.^{6–8} The critical roles of the ECS in adipose homeostasis and energy balance are underscored by the remarkable anti-obesity effects produced, in pre-clinical studies and clinical trials, by globally or peripherally active CB₁ receptor inverse agonists and neutral antagonists.⁹ The pharmacological efficacy of these agents is primarily due to their ability to stimulate lipolysis, energy dissipation, and fatty

acid oxidation by countering energy-conserving endocannabinoid signals in adipose, liver, and other organs.^{9,10}

The ECS is the molecular target of the phytocannabinoid, Δ^9 -tetrahydrocannabinol (THC),¹¹ which accumulates in fat depots at concentrations that can fully engage local CB₁ receptors.^{12,13} Given the receptors' roles in adipose function, this tissue distribution predicts that persons who regularly use cannabis should exhibit, all else being equal, body mass index (BMI) values higher than the general population. However, the opposite appears to be the case. Cross-sectional and longitudinal studies have consistently reported lower BMI in healthy cannabis users compared with non-users, as well as inverse associations of cannabis use with BMI, waist circumference, and other cardiometabolic risk factors.^{14–29} These studies are further supported by the prospective National Epidemiologic Survey on Alcohol and Related Conditions (NESARC), whose sampling was devised to yield representative estimates for the adult US population.²¹ The metabolic phenotype of habitual cannabis users is all the more paradoxical because one of the drug's most iconic effects is the stimulation of hedonic high-calorie food intake

(the munchies),^{30–32} which does not undergo noticeable tolerance with continued non-medical use of the drug.^{19,33}

Regular cannabis consumption often starts in adolescence. For example, in a cohort of adult individuals who successfully recovered from cannabis use disorder,³⁴ continuous drug use began between 15 and 17 years of age.³⁵ This pattern suggests that the metabolic phenotype of habitual adult users might reflect, at least in part, enduring molecular changes initiated by inappropriate CB₁ receptor activation during teenage years. Consistent with this idea—and offering new insights into the contribution of the ECS to adipose homeostasis—we report now that daily exposure to low-dose THC during adolescence causes, in male mice, a lasting metabolic state characterized by smaller fat mass, greater lean mass, increased utilization of fat as fuel, partial resistance to diet-induced obesity and dyslipidemia, impaired thermoregulation, and blunted cold- and β -adrenergic receptor-stimulated lipolysis. Multi-omics and morphological investigations of the adipose organ show that this state is associated with a broad transcriptional dysregulation that results, among other changes, in a striking ectopic expression of proteins normally found in muscle.

RESULTS

Adolescent THC exposure reduces body weight gain via activation of CB₁ receptors in differentiated adipocytes

Figures 1A and 1B illustrate the body weight trajectory of adolescent male and female mice (postnatal day [PND] 30–43) treated once daily with a dose of THC (5 mg/kg, intraperitoneal [i.p.]) that, in male mice of this age, produces only a modest decrease in body temperature ($\sim 1^\circ\text{C}$) and no change in motor activity or food intake.^{13,36} THC-exposed mice of both sexes gained significantly less weight than did control animals treated only with vehicle. Subsequent analyses, which were focused on males, showed that this effect could not be attributed to changes in growth rate (Figure 1C; head length, tail length, and femur length and weight are shown in Figures S1A–S1D), locomotor activity (Figure 1D; circadian data are shown in Figure S1E), food intake (Figure 1E; meal patterns are shown in Figures S1F1–6), or nutrient absorption (Figure 1F). Moreover, there were no statistically detectable differences in intestinal microbiome composition between the two groups (Figure 1G; Table S1).

Three datasets indicate that adolescent THC exposure dampened weight gain through activation of CB₁ receptors in the adipose organ, a major site of THC accumulation.^{12,13} First, the effect of THC was prevented by co-administration of either the global CB₁ inverse agonist AM251 (1 mg/kg, i.p.) or the peripherally restricted CB₁ neutral antagonist AM6545 (3 mg/kg, i.p.) (Figure 1H). Neither agent affected weight gain when administered alone (Figure 1H). Second, the global CB₂ inverse agonist AM630 (1 mg/kg, i.p.) did not affect the response to THC (Figures S1G and S1H). Third, adolescent THC treatment did not reduce weight gain in male conditional knockout mice in which CB₁ was deleted postnatally in differentiated white and brown adipocytes (Figure 1I). The mutants were generated by crossing CB₁-floxed mice with transgenic AdipoqCreERT2 mice—which express Cre recombinase under the control of the promoter for the differentiated adipocyte gene *Adipoq*^{37,38}—followed by tamoxifen-induced recombination on

PND14–18.³⁹ Adipose-specific CB₁ deletion was confirmed by RT-PCR (Figure 1J). Last, and importantly, the same THC regimen that blunted weight gain during adolescence had no such effect when carried out in young adulthood (PND70–PND83) (Figure 1K). The results indicate that daily exposure to low-dose THC reduces body weight gain in adolescent male mice through a developmentally regulated mechanism that depends on CB₁ receptor activation in differentiated adipocytes.

Adolescent THC exposure modifies adult energy metabolism and body mass composition

Consistent with the observed reduction in weight accrual, metabolic studies at the end of the treatment period (PND44) revealed that male THC-exposed mice exhibited, compared with vehicle controls, heightened energy expenditure (EE) and reduced respiratory exchange ratio (RER) during both dark (active) and light (inactive) phases of the 24-h cycle (Figures 2A and 2B; EE data not normalized by body weight, and individual body weight values reported in Figures S2A and S2B). Magnetic resonance imaging (MRI) analyses showed that relative lean mass, fat mass, and water content were not affected by the treatment (Figure 2C; water content is shown in Figure S2C). However, accounting for the animals' reduced weight gain, we observed significant decreases in absolute lean mass and water content along with a trend toward decreased fat mass (Figures S2D–S2F). Body weight returned to normal within approximately 10 days of treatment termination (Figure 2D).

By young adulthood (PND70), when adipose THC content had fallen below the quantification limit of our mass spectrometry assay (0.6 pmol on column) (Figure 2E), a new set of changes in energy metabolism and body mass composition had emerged. Both EE and RER were attenuated in THC-treated mice—the former throughout the 24-h period (Figure 2F; EE data not normalized by body weight and individual body weight values are reported in Figures S2G and S2H) and the latter only during the dark phase (Figure 2G). In addition, relative (percent body weight) fat mass and adipocyte area in epididymal WAT were decreased, whereas relative lean mass was increased in the THC group compared with control (Figures 2H and 2I). Water content was not affected (Figure S2I). Similarly, microbiome composition (Figure S2J) and blood chemistry profile (Table S2) were not changed by THC treatment. The data suggest that adolescent exposure to low-dose THC caused in male mice two temporally distinct sets of metabolic modifications (summarized in Table S3). At PND44, when the adipose organ still contained bioactive concentrations of the drug (~ 120 nM in WAT; Figure 2E), body weight was blunted (likely due to reduced muscle and water content), EE was elevated, and RER was reduced. After THC had been completely eliminated from the body and the animals had reached young adulthood, a different metabolic state took effect in which average body weight returned to normative values, while fat mass, white adipocyte area, EE, and RER were decreased and lean mass was increased.

Persistent functional consequences of adolescent THC exposure

To better understand the lasting consequences of adolescent THC exposure on energy balance, we treated adolescent male

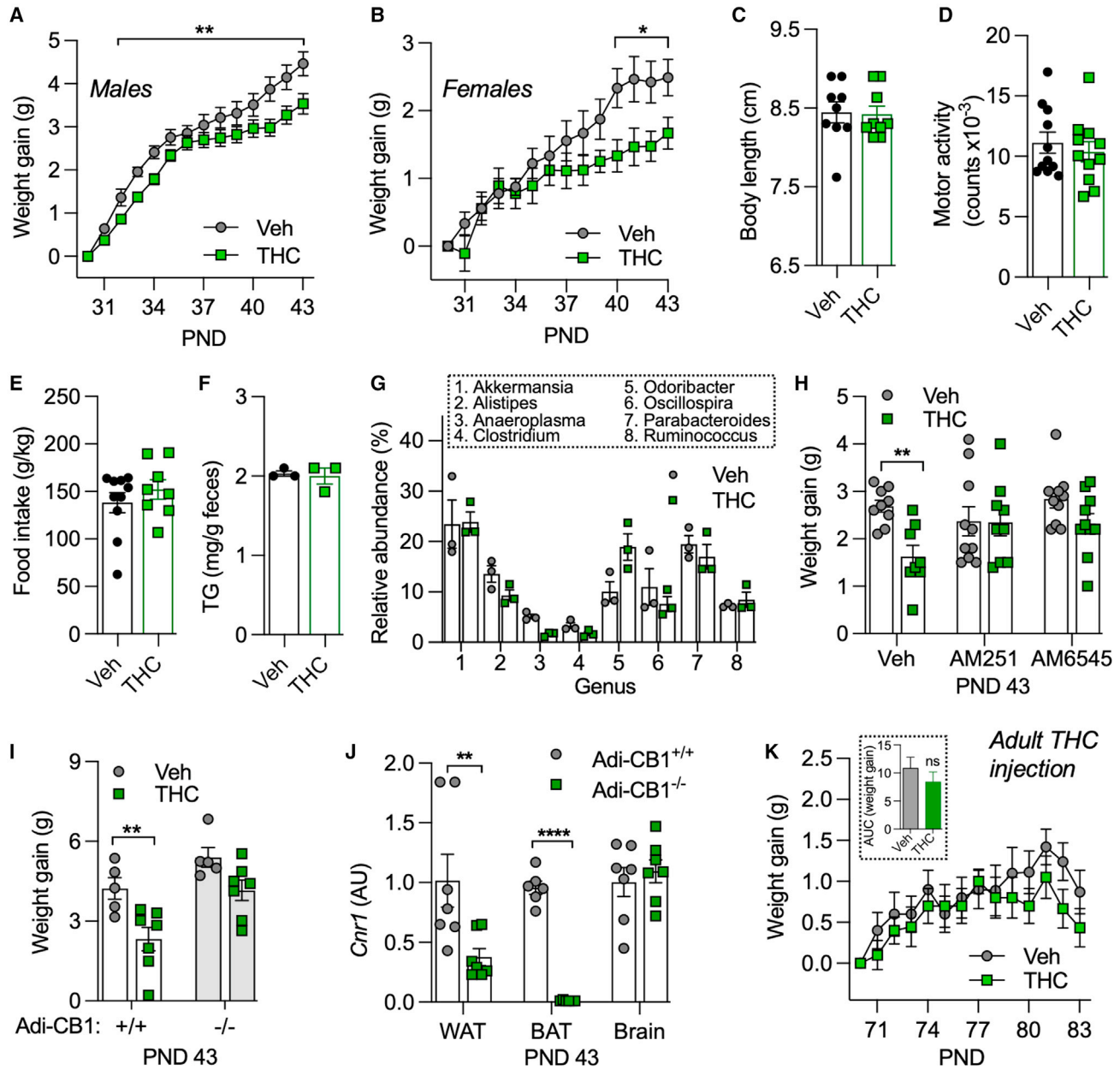


Figure 1. Adolescent THC exposure attenuates body weight gain via activation of CB₁ receptors in adipocytes

(A and B) Effects of adolescent administration of THC (green squares) or vehicle (gray circles) on body weight gain in (A) male and (B) female mice (n = 30 and 9 per group, respectively).

(C–G) In males, the treatment did not affect (C) growth rate (n = 9); (D) motor activity (n = 11); (E) cumulative food intake (n = 8–10); (F) nutrient absorption, expressed as mg of total triglycerides (TG) per g of feces (n = 3 cages of 4 mice each); or (G) intestinal microbiome composition (n = 3 cages). Displayed are bacterial genera that represent >1% of the total microbiome community.

(H) The global CB₁ inverse agonist AM251 (1 mg/kg) or the peripheral CB₁ neutral antagonist AM6545 (3 mg/kg) prevented THC's effect on body weight gain, assessed on PND43 (n = 8–10).

(I) Adolescent THC treatment did not alter weight gain in adipocyte-selective *Cnr1*^{-/-} (*Adi-CB1*^{-/-}) mice.

(J) *Cnr1* mRNA levels in white adipose tissue (WAT), brown adipose tissue (BAT), and the brains of male *Adi-CB1*^{-/-} and *Adi-CB1*^{+/+} mice (n = 5–7).

(K) Subchronic THC treatment did not affect weight gain in young adult (PND70–83) male mice (n = 9–10).

AUC, area under the curve; ns, not significant. *p < 0.05, **p < 0.01, and ****p < 0.0001, two-way ANOVA followed by Tukey post hoc test (A and B), Student's t test (C–F, J, and inset in K), mixed-effects ANOVA followed by Bonferroni's post hoc test (H and K), or mixed-effects ANOVA followed by Bonferroni's post hoc test (I).

Statistics for microbiome analyses are described under [STAR Methods](#).

See also [Figures S1](#) and [S2](#) and [Table S1](#).

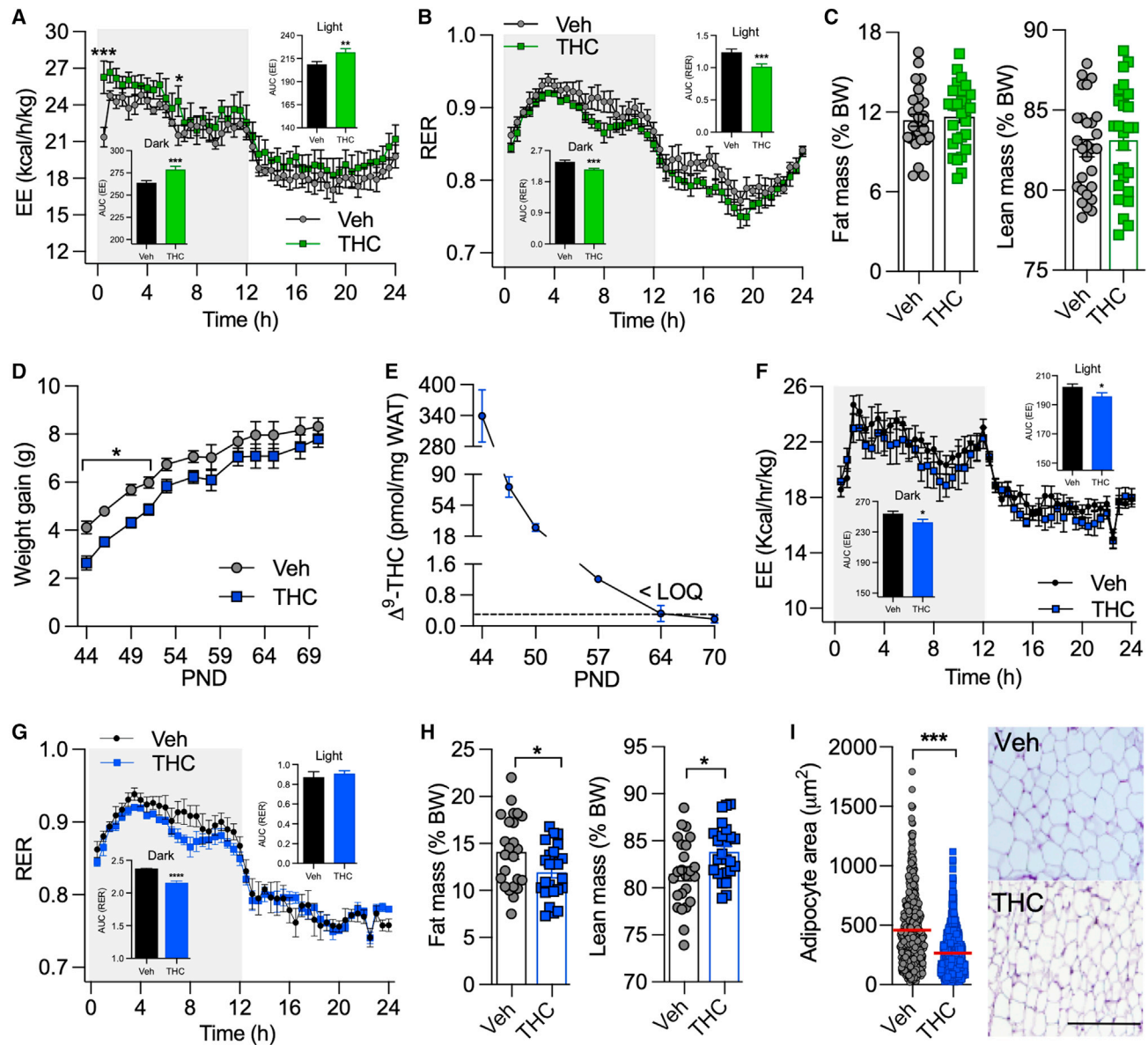


Figure 2. Adolescent THC exposure modifies energy metabolism and body mass composition in adulthood

(A–C) Residual effects of adolescent administration of THC (green squares) or vehicle (gray circles) in male mice on (A) energy expenditure (EE, $n = 4$ per group), (B) respiratory exchange ratio (RER) ($n = 4$), and (C) percent fat (left) and lean (right) mass ($n = 30$). Measurements were made at PND44. AUC, area under the curve. (D) Body weight trajectory after THC treatment termination ($n = 15$ –43).

(E) Time course of THC concentration in epididymal WAT following treatment termination ($n = 3$ –4); dotted line indicates limit of quantification (LOQ).

(F–I) Persistent effects of adolescent administration of THC or vehicle on (F) EE ($n = 4$), (G) RER ($n = 4$), (H) relative (percent body weight) fat (left) and lean (right) mass ($n = 24$ –26), and (I) white adipocyte area (epididymal fat) ($n = 557$ and 994 cells for vehicle and THC, respectively, measured in three randomly selected regions [$200 \times 200 \mu\text{m}^2$] from each mouse [$n = 3$ mice per group]).

Scale bars, $100 \mu\text{m}$. Male young-adult (PND70) mice were used in these experiments. * $p < 0.05$, ** $p < 0.01$, *** $p < 0.001$, and **** $p < 0.0001$, two-way ANOVA followed by Tukey post hoc test (A, B, F, and G), Student's *t* test (C, H, I, and insets in A, B, F, and G), or mixed-effects ANOVA followed by Bonferroni's post hoc test (D and E).

See also [Figures S2](#) and [S3](#) and [Tables S2](#) and [S3](#).

mice with the drug or its vehicle and, when the animals reached PND57, gave them access to a high-fat diet (HFD, 60% kcal fat) for 10 weeks. THC-exposed animals gained significantly less weight than did vehicle controls (Figure 3A), even though the two groups did not differ in food intake, motor activity, or nutrient absorption (Figures 3B–3D). Further analyses revealed that HFD-

fed mice that had received THC exhibited, compared with controls, (1) higher dark-phase EE and lower light-phase RER (Figures 3E and 3F; EE data not normalized by body weight, and individual body weight values reported in Figures S2K and S2L); (2) lower percent fat mass and epididymal adipocyte area (Figures 3G and 3H); (3) higher percent lean

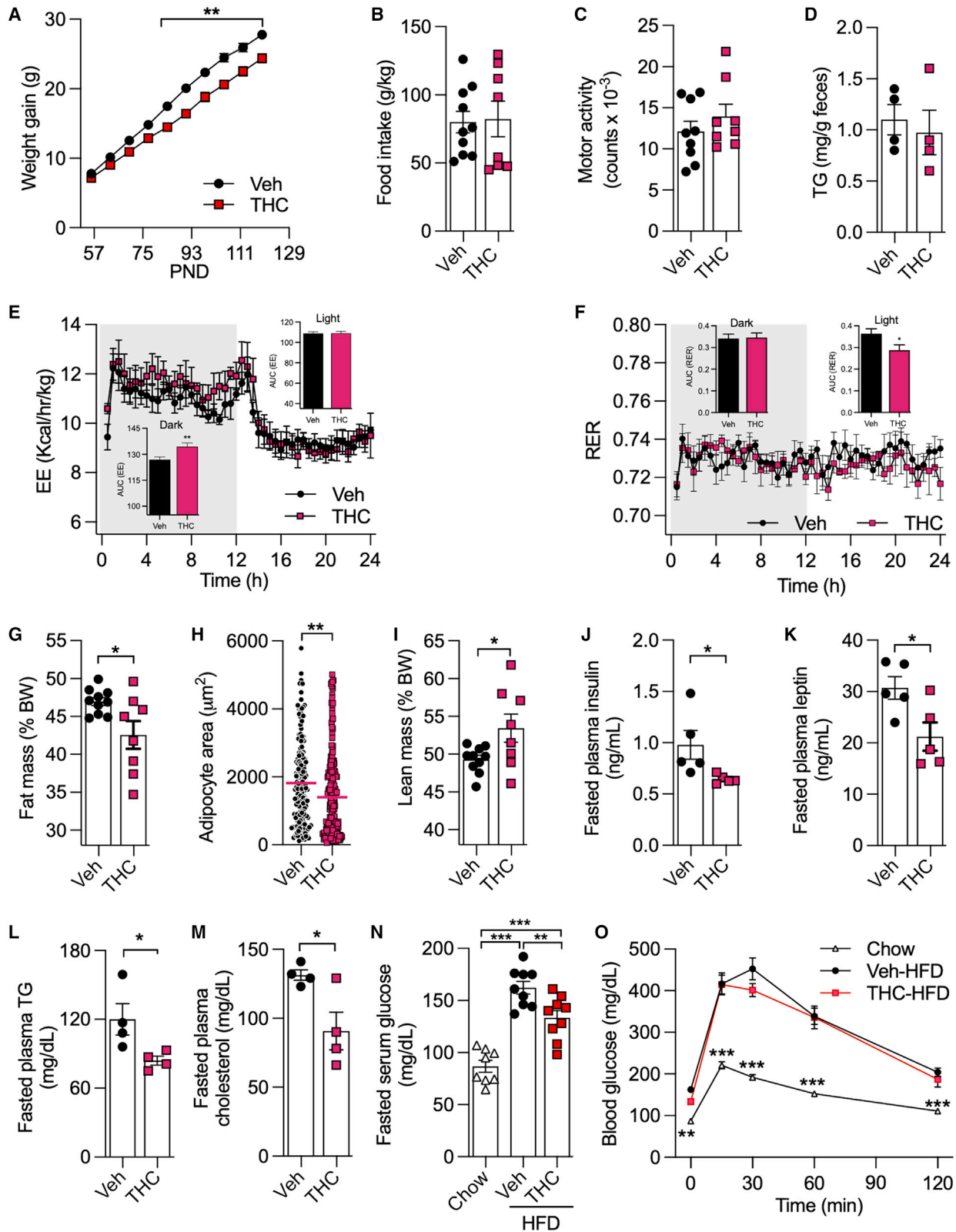


Figure 3. Adolescent THC exposure attenuates body weight gain and dysmetabolic responses in adult HFD-fed male mice

Persistent effects of adolescent administration of THC (red squares) or vehicle (filled circles) on metabolic responses to HFD.

(A) Body weight gain (n = 8–11 per group).

(legend continued on next page)

mass (Figure 3I); (4) lower fasted plasma insulin, leptin, triglycerides, cholesterol, and serum glucose (Figures 3J–3N); and (5) no change in relative water content (Figure S2M; phenotype summarized in Table S3). Glucose handling did not differ between the two groups (Figure 3O).

In separate cohorts of mice, we assessed the acute adaptive response to low ambient temperature, which simultaneously stimulates thermogenesis in BAT and lipolysis in WAT.³ Under baseline conditions, core body temperature was $\sim 1^{\circ}\text{C}$ higher in THC-exposed than control animals (Figure 4A). After transfer to a cold room, body temperature decreased in both groups and plateaued 2 h later at a significantly higher level in THC-treated mice relative to controls (Figure 4B). THC-exposed animals also exhibited blunted cold-induced release of free fatty acids (FFAs) into the circulation, relative to controls (Figure 4C). Locomotor activity in an unfamiliar environment did not differ between the two groups (Figure 4D). We also examined whether adolescent THC treatment modified the response to a selective β_3 -adrenergic receptor agonist (CL316,243, 1 mg/kg, i.p.). The compound increased body temperature and plasma FFA concentrations in vehicle- but not THC-treated mice (Figures 4E and 4F). Collectively, the results indicate that adolescent exposure to low-dose THC produces in male mice a lasting metabolic state characterized by lower fat mass, higher lean mass, partial resistance to diet-induced obesity and dyslipidemia, altered thermogenesis, and blunted lipolytic response to physiological and pharmacological stimuli.

Effects of adolescent THC exposure on endocannabinoid signaling in the adult adipose organ

We next asked whether ECS downregulation in white and brown adipocytes, which is expected to decrease lipogenesis and stimulate thermogenesis,^{6–8} might underpin the persistent metabolic state induced by adolescent THC exposure. Countering this possibility, however, analyses of BAT and WAT from THC-treated and control mice at PND70 revealed no difference in the expression of critical ECS components, including CB₁ receptor mRNA and protein (Figures S3A and S3B), as well as mRNAs encoding for the 2-AG-metabolizing enzymes, diacylglycerol lipase- α (DGL- α) and monoglyceride lipase (MGL) (Figures S3C and S3D). Transcription of N-acyl-phosphatidyl-

ethanolamine phospholipase D (NAPE-PLD) and fatty acid amide hydrolase (FAAH)—which produce and hydrolyze, respectively, anandamide and other fatty acyl ethanolamides^{1,2}—was increased in WAT, but not in BAT (Figures S3E and S3F). 2-AG levels were unaffected in BAT and WAT (Figure S3G and S3H), while small but statistically significant changes were observed in the levels of anandamide (up in WAT, down in BAT) (Figures S3G and S3H). Overall, the limited impact of adolescent THC administration on the adult ECS is unlikely to account for the substantive metabolic alterations caused by the drug.

Adolescent THC exposure disrupts gene transcription in the adult adipose organ

RNA sequencing experiments provided unexpected insights into the molecular events that might underpin such effects. Transcriptome datasets from interscapular BAT and epididymal WAT of vehicle- and THC-treated male mice were readily distinguishable by principal component analysis (Figures 5A and 5B). The total number of genes differentially expressed between the two groups was 2,985 (1,443 up) in BAT and 3,446 (1,617 up) in WAT (Figures 5C and 5D). Gene ontology (GO) annotation revealed, in both compartments, a striking overrepresentation of genes encoding for contractile proteins that are normally expressed in muscle and heart (Figures 5E and 5F; Table S4). GO categories most affected were contractile fiber (GO:0043292; adjusted p value [padj] = $3.16\text{e-}49$ and $1.41\text{e-}15$ for BAT and WAT, respectively), myofibril (GO:0030016, padj = $3.13\text{e-}48$ and $1.41\text{e-}15$), sarcomere (GO:0030017, padj = $6.56\text{e-}48$ and $3.43\text{e-}15$), and contractile fiber part (GO:0044449, padj = $3.16\text{e-}49$ and $7.67\text{e-}15$). Conversely, genes involved in mitochondrial respiration and protein synthesis were underrepresented, including mitochondrial protein complex (GO:0098798, padj = $1.54\text{e-}30$ and $1.19\text{e-}56$ for BAT and WAT, respectively), mitochondrial inner membrane (GO:0005743, padj = $2.62\text{e-}33$ and $9.89\text{e-}47$), and mitochondrial matrix (GO:0005759, padj = $1.88\text{e-}19$ and $3.77\text{e-}43$) (Figures 5E and 5F; Table S4). Little or no change was seen in GO categories encompassing macrophage activation, innate immunity, and inflammation (Table S4), which are overrepresented in adult rat adipose tissue after repeated exposure to THC.⁴⁰ The effect of THC was both organ-specific and

(B) Cumulative food intake (n = 8–10).

(C) Motor activity (n = 8–9).

(D) Nutrient absorption expressed as mg of total triglycerides (TG) per g of feces (n = 4 cages with 4 mice each).

(E) EE (n = 4).

(F) RER (n = 4).

(G) Percent fat mass (n = 8–10).

(H) White adipocyte area (epididymal fat) (n = 275 and 341 cells for Veh and THC, respectively, measured in six randomly selected regions [$200 \times 200 \mu\text{m}^2$] from each mouse [n = 4 mice per group]).

(I) Percent lean mass (n = 8–10).

(J) Fasting plasma insulin (n = 5).

(K) Fasting plasma leptin (n = 5).

(L) Fasting plasma triglycerides (n = 4).

(M) Fasting plasma total cholesterol (n = 4).

(N) Fasting serum glucose (n = 8–9).

(O) Glucose tolerance test (n = 8–9).

AUC, area under the curve. Male adult (PND130) mice were used in these experiments. *p < 0.05, **p < 0.01, ***p < 0.001, mixed-effects ANOVA followed by Bonferroni's post hoc test (A and O), Student's t test (B–D, G–N, and insets in E and F), or two-way ANOVA followed by Tukey post hoc test (E and F). See also Figure S2 and Table S3.

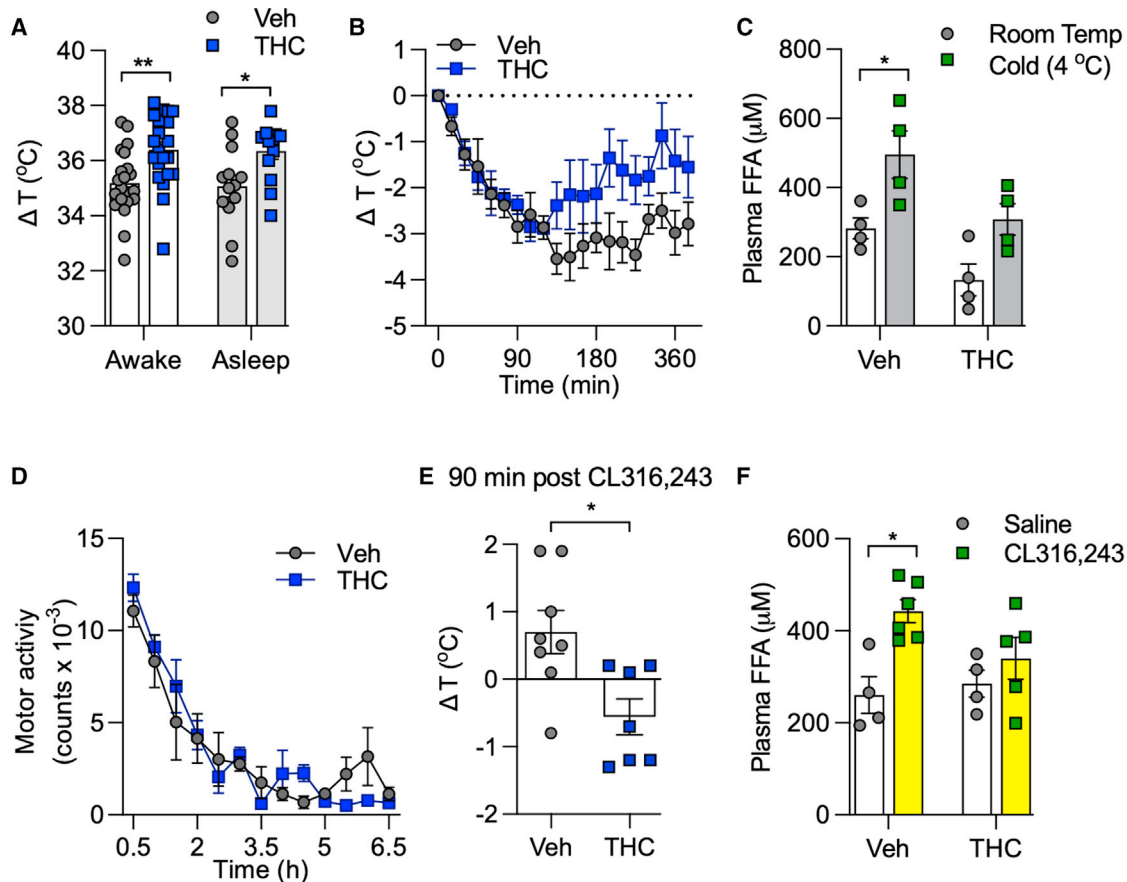


Figure 4. Adolescent THC exposure modifies thermoregulation and lipolysis in adulthood

(A) Effects of adolescent administration of THC (squares) or vehicle (circles) on core body temperature (T) in awake (n = 21) or asleep (n = 13) male mice kept at room temperature.
 (B) Time course of body temperature change (ΔT) in THC- and vehicle-treated mice kept at 0°C–4°C for 6.5 h (n = 4 each). Two-way ANOVA followed by Bonferroni post hoc test revealed a significant time \times treatment interaction effect (p = 0.005).
 (C) Plasma free fatty acid (FFA) concentrations in mice treated with THC or vehicle and kept at room temperature (circles) or 0°C–4°C for 6.5 h (squares) (n = 4 each).
 (D) Motor activity of mice treated with THC (blue squares) or vehicle (gray circles) and kept at 0°C–4°C for 6.5 h (n = 4 each).
 (E) Effects of β_3 -adrenergic agonist CL316,243 (1 mg/kg, i.p.) on core body temperature in THC- (squares) and vehicle-treated (circles) mice (n = 7–8 each).
 (F) Effects of CL316,243 (squares) or saline (circles) on plasma FFA in mice treated with THC or vehicle and kept at room temperature.
 Experiments were conducted on young-adult (PND70) male mice. *p < 0.05 and **p < 0.01, Student's t test (A and E), two-way ANOVA followed by Bonferroni's post hoc test (B and D) or mixed-effects ANOVA followed by Bonferroni's post hoc test (C) and one-way ANOVA followed by Tukey post hoc test (F).

developmentally regulated. Indeed, parallel analyses of skeletal muscle (hindlimb quadriceps) at PND70 revealed a more limited (Figures 5G and 5H) and distinct (Figure 5I) set of transcriptional alterations, which included downregulation of many of the sarcomere-associated genes that were elevated in BAT and WAT. Similarly, the impact of adult THC treatment (PND70–83) on gene transcription in BAT and WAT, assessed at PND110, was much more modest than the one produced by adolescent exposure and did not include muscle-related GO categories (Figures S4A–S4D).

Closer inspection of the data from male mice treated with THC in adolescence, showed that transcription of multiple genes encoding for sarcomere constituents—e.g., titin (*Ttn*); myosin heavy chain (*Myh*) 1, 2, and 7; myosin light chain 3 (*Myl2*); troponin 1 (*Tnni2*); and troponin T (*Tnnt3*)—as well as enzymes primarily found in muscle—e.g., enolase 3 (*Eno3*) and

sarco(endo)plasmic reticulum calcium ATPase 1 (*Atp2a1*)—was markedly increased in BAT and, to a lesser extent, WAT (Figure 6A). Conversely, transcription of nuclear-encoded genes involved in mitochondrial respiration—including *Atp5* (ATP synthase subunit 5) and *Ndufa* (NADH:ubiquinone oxidoreductase), two components of respiratory chain complex I—was suppressed (Figure 6B). It is worth noting, however, that expression of the master regulator of mitochondrial biogenesis, *Pgc1a* (peroxisome proliferator-activated receptor- γ coactivator-1 α), was enhanced in both BAT and WAT (Figure S4E), while transcription of various genes that are essential for adipose organ function was either unaffected (peroxisome proliferator-activated receptor- γ [*Pparg*]) or differentially regulated in the two compartments (PR/SET domain 16 [*Prdm16*], β -adrenergic receptor [*Adrb3*], uncoupling protein 2 [*Ucp2*]: down in BAT, up in WAT; *Ucp1*: up in BAT, unchanged in WAT; *Ucp3*: unchanged

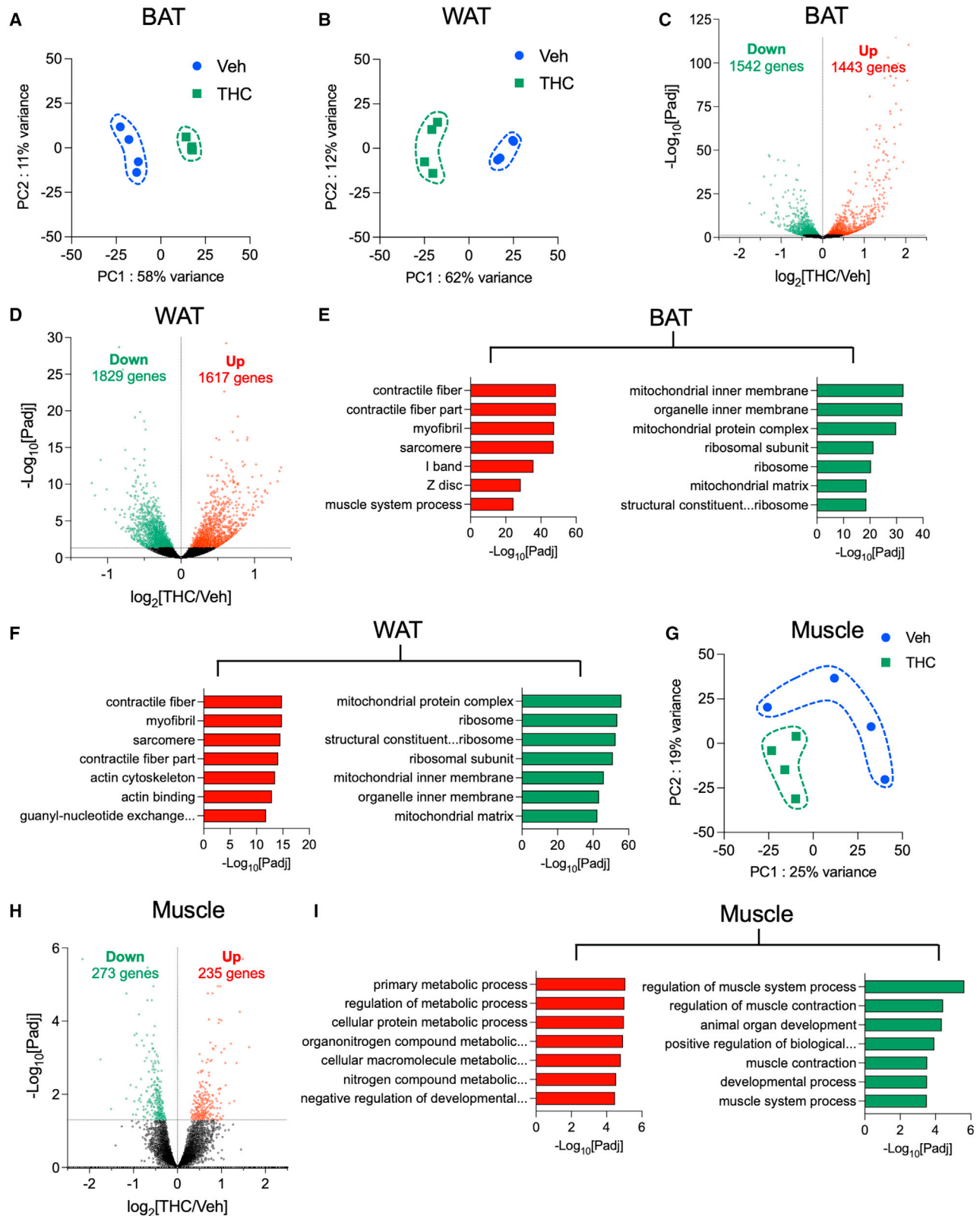


Figure 5. Adolescent THC exposure disrupts gene transcription in adipose organ in adulthood

(A–C) Principal component analysis of transcriptome datasets from (A) BAT, (B) WAT, and (C) skeletal muscle of male mice treated in adolescence with THC (green squares) or vehicle (blue circles).

(legend continued on next page)

in BAT, up in WAT) (Figures S4F–S4K). Confirming the organ-specificity of THC's effects, a distinct and partially opposite set of transcriptional modifications was evident in skeletal muscle, where many genes implicated in sarcomere structure/function, calcium transport, and cellular respiration were downregulated in THC-exposed relative to control animals (Figures 6A and 6B). Thus, adolescent THC treatment produces a complex array of enduring transcriptional abnormalities in the mouse adipose organ—including ectopic expression of genes encoding for sarcomere proteins, and suppression of genes involved in mitochondrial respiration.

Adolescent THC exposure alters protein expression in the adult adipose organ

Consistent with the transcriptomic data, untargeted mass spectrometry analyses revealed substantial proteomic alterations in the adipose organs of adult male mice that had received THC in adolescence. Statistically detectable differences ($p < 0.05$) between THC-exposed and control animals were observed in both BAT (102 proteins, 75 up) and WAT (44 proteins, 6 up) (Figure S5A and S5B). In the BAT of THC-treated mice, STRING analysis⁴¹ of proteins with high fold-increases revealed a marked enrichment (strength > 1.9) in categories related to muscle components (Figure 6C; Table S5). Affected proteins included essential sarcomere constituents, such as titin (~30-fold increase), troponin (~2-fold), and myosin (~1.5-fold) (Figure 6D)—whose gene transcription was enhanced (Figure 6A)—but also proteins involved in mitochondrial respiration, such as NADH dehydrogenase 1 α -subcomplex subunit 3 and 5 (NDUA3 and 5), and cytochrome c oxidase subunit 5A (COX5A) (Figure 6D)—whose transcription was suppressed (Figure 6B). Immunohistochemical studies of intrascapular BAT showed that, in control mice, immunoreactive titin was primarily localized to vascular smooth muscle (Figure 6E). By contrast, intense titin immunoreactivity was observed in brown adipocytes of animals treated with THC (Figure 6F). Select BAT proteins downregulated by THC are reported in Figures S5C and S5D. Additional proteins overrepresented or underrepresented in the BAT of THC-treated mice are listed in Tables S5 and S6, respectively. Proteins exclusively detected in THC-exposed BAT, 160 in total, are reported in Table S7.

THC treatment produced fewer proteomic changes in WAT than it did in BAT. Nevertheless, the levels of three muscle-associated proteins—titin, myosin 1B, and myosin 9—as well as levels of proteins involved in intracellular trafficking (sorting nexin 1 [SNX1]) and transmembrane receptor function (arrestin beta-1 [ARRB1]), among others, were also noticeably increased in this compartment (Figures 6G and 6H). Select WAT proteins downregulated by THC are reported in Figures S5E and S5F. Additional proteins overrepresented or underrepresented in WAT of THC-treated mice are reported in Tables S5 and S6, respectively. Proteins only detectable in THC-exposed WAT, a total of 288, are shown in Table S7.

Adolescent THC exposure modifies amino acid metabolism in adult BAT

Targeted metabolomic studies revealed significant upregulation of several metabolites in the BAT of THC-exposed male mice (Figures 7A–7C). Unexpectedly, metabolites related to energy production pathways, such as glycolysis, the tricarboxylic acid cycle, and the pentose phosphate pathway, were not affected by THC treatment (Figures S6A–S6C). Nucleotides were also largely unchanged (Figure S6D). By contrast, essential and non-essential amino acids, as well as N-acetylated amino acids, were elevated in the THC group (Figures 7D–7F), which is suggestive of enhanced anabolic processing. Consistent with this idea, we found that the NADPH/NADP⁺ ratio was significantly decreased (Figure 7G), possibly due to increased NADPH consumption for protein synthesis. The NADH/NAD⁺ ratio was unchanged (Figure 7G). Interestingly, no significant metabolomic alterations were seen in WAT (Figures S6E–S6K), in which the transcriptomic and proteomic response to THC was also less pronounced. Finally, observations by transmission electron microscopy did not identify any significant ultrastructural difference in brown and white adipocytes from THC-exposed and control mice (Figures S7A–S7C). Furthermore, in BAT, no differences were seen in the density of parenchymal noradrenergic (tyrosine hydroxylase-positive) fibers or lipid droplet size (Figure S7D).

DISCUSSION

This study examined whether daily adolescent exposure to the intoxicating constituent of cannabis, THC, alters energy balance and adipose organ function in adult life. The question is important for two reasons. First, many teenagers use cannabis regularly and continue doing so until they become adults.^{35,42} Second, epidemiological surveys have found robust associations between habitual cannabis use and alterations in metabolic function.^{15–29} Understanding the molecular underpinnings of such alterations and their possible link to adolescent exposure is necessary to inform evidence-based prevention and guide future research.

In the present experiments, a THC administration regimen that approximates daily human use of a low psychoactive dose of the drug^{13,36} dampened body weight gain in adolescent mice of both sexes. When treatment was stopped, THC-treated male mice (on which we focused subsequent experiments) expended more energy than did vehicle-treated controls and, by the time they reached adulthood, transitioned to a different metabolic state, whose features included normal body weight, decreased fat mass and white adipocyte area, increased lean mass, partial resistance to diet-induced obesity and dyslipidemia, abnormal thermogenesis, and blunted stimulus-induced lipolysis. Utilization of fat as fuel was increased during the dark (active) phase of the 24-h cycle, but EE could be either lower or higher than control, depending on whether the mice were fed normal chow or an

(D–F) Volcano plots showing genes differentially expressed ($p_{\text{adj}} < 0.05$) in (D) BAT, (E) WAT, and (F) skeletal muscle. Red, upregulated; green, downregulated; black, unchanged ($p_{\text{adj}} > 0.05$).

(G–I) GO categories showing highest enrichment in (G) BAT, (H) WAT, and (I) skeletal muscle. Ranking is according to $-\log_{10} p_{\text{adj}}$ value. Top, upregulated genes (red bars); bottom, downregulated genes (green bars).

Experiments were conducted on young-adult (PND70) male mice. $n = 3–4$ per group. Statistical analyses are described under STAR Methods. See also Figure S4 and Table S4.

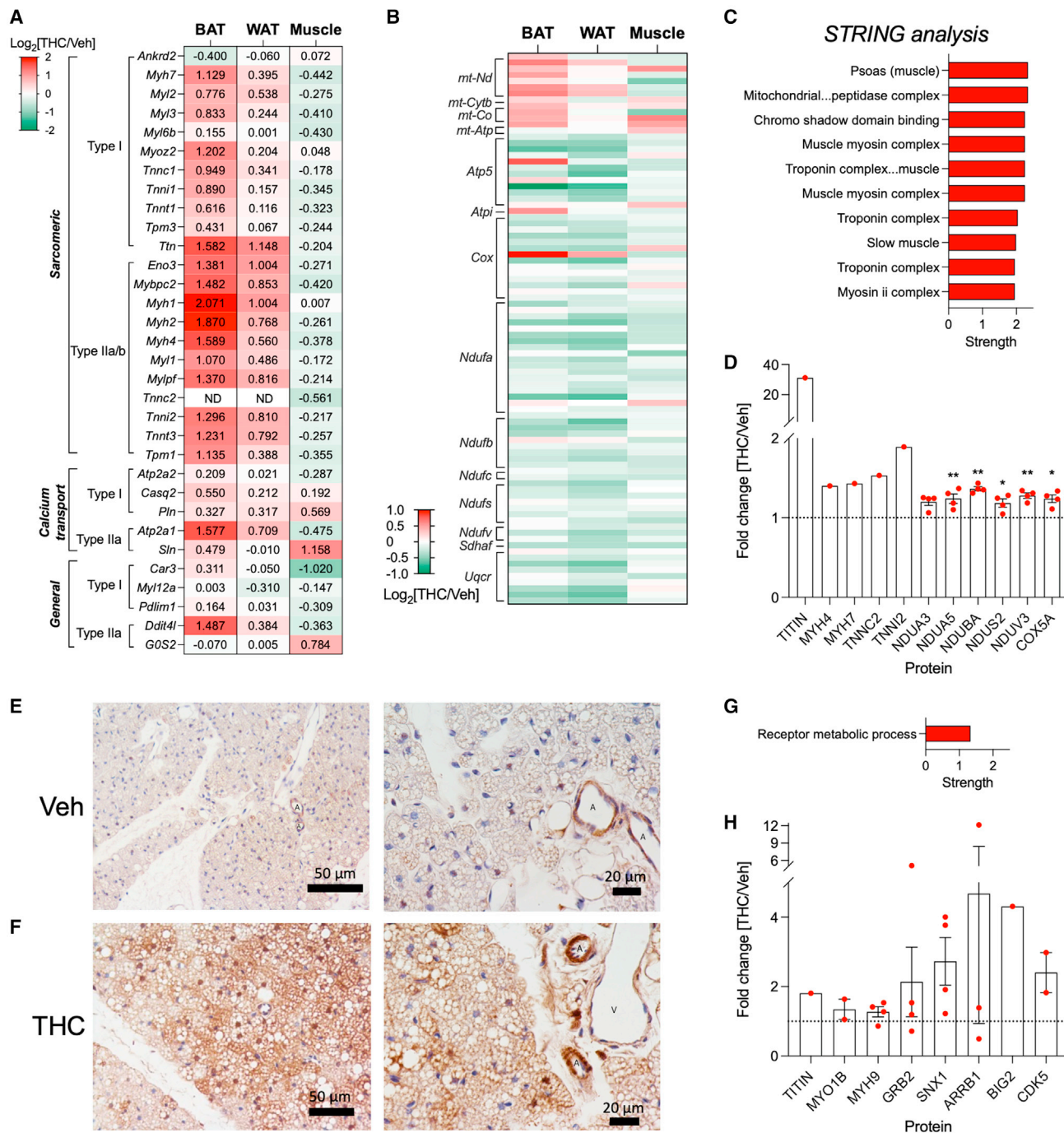


Figure 6. Adolescent THC exposure causes ectopic expression of muscle-associated proteins in the adult adipose organ

(A and B) Heatmaps showing the effects of adolescent THC treatment in male mice on the transcription of select (A) muscle-associated genes, and (B) genes involved in mitochondrial function and oxidative phosphorylation. In (A), numbers represent the $\log_2[\text{THC}/\text{Veh}]$ value for each gene.

(C and D) Untargeted proteomics analyses in BAT: (C) STRING annotation of upregulated proteins in THC- versus vehicle-treated mice. Protein term IDs showing significant enrichment ($p_{\text{adj}} < 0.05$) were identified and those with strength > 1.0 are ranked in figure.

(D) Fold changes in abundance of select proteins upregulated by THC treatment.

(E and F) Immunohistochemical localization of muscle-associated protein, titin, in brown adipocytes of (E) vehicle-treated and (F) THC-treated mice. A, arteriole; V, venule. Scale bars, left, 50 μm ; right, 20 μm (left and right panels are from different tissue sections).

(G and H) Untargeted proteomics analyses in WAT. (G) STRING annotation of upregulated proteins in THC- versus vehicle-treated mice. (H) Fold changes in abundance of select proteins upregulated by THC treatment.

Experiments were conducted on young-adult (PND70) male mice. * $p < 0.05$ and ** $p < 0.01$ by Student's *t* test ($n = 4$) (D and H).

See also [Figure S5](#) and [Tables S5](#), [S6](#), and [S7](#).

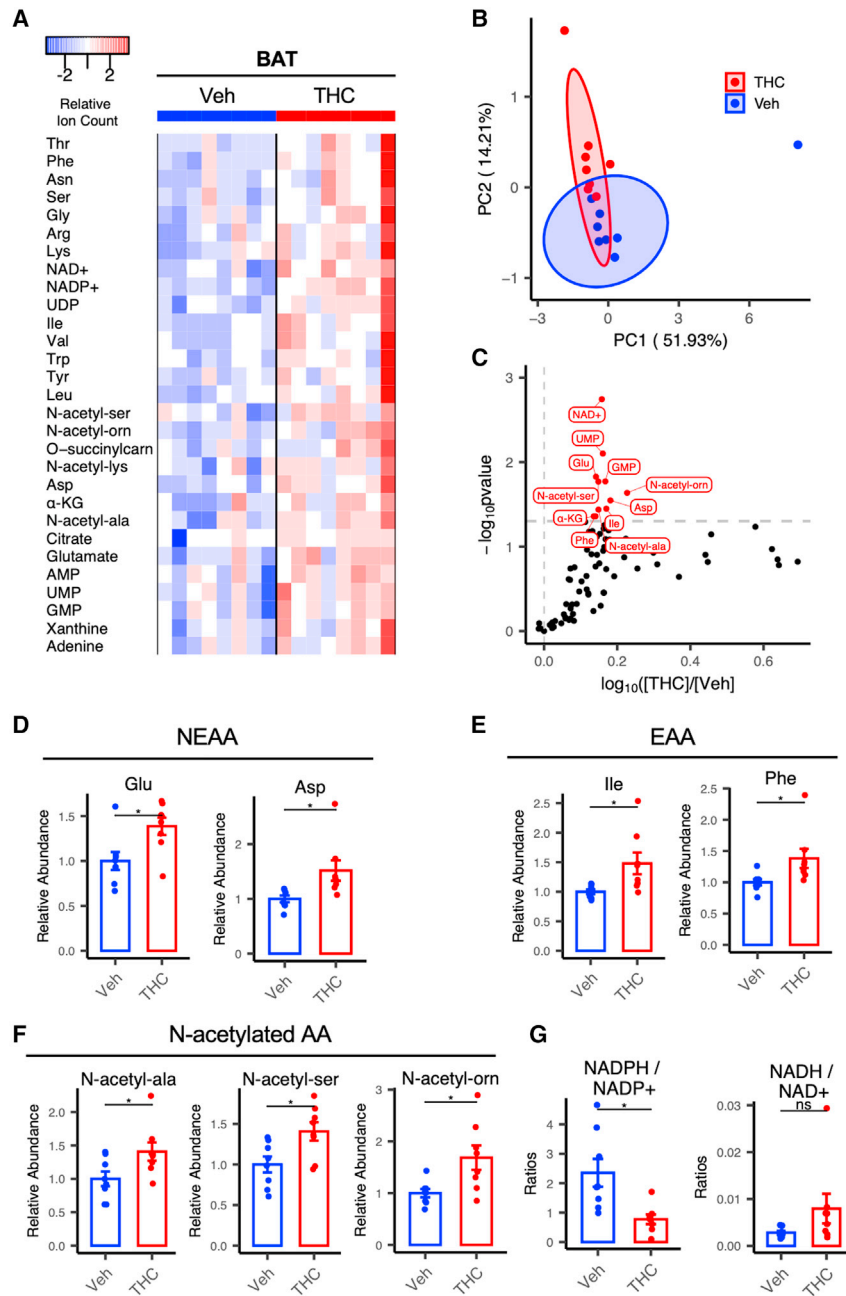


Figure 7. Adolescent THC exposure modifies amino acid metabolism in BAT in adulthood

(A) Heatmap illustrating the effects of adolescent THC treatment on select intermediate metabolites in BAT. Top 29 compounds with highest statistical significance are shown (Student's *t* test, *n* = 8 per group).

(B) Principal component analysis of top 29 compounds.

(C) Volcano plot showing changes in individual metabolites (\log_{10} of THC/Veh).

(D–F) Relative abundance of the indicated metabolites.

(G) NADPH/NADP⁺ and NADH/NAD⁺ ratios.

Experiments were conducted on young-adult (PND70) male mice. **p* < 0.05 by Student's *t* test (*n* = 8).

See also Figures S6 and S7.

Our findings indicate that CB₁ receptor activation in differentiated adipocytes mediates the effect of adolescent THC exposure on body weight accrual. Supporting this conclusion, we found that the response to THC in male mice (1) was prevented by co-treatment with a global CB₁ inverse agonist (AM251) or a peripheral CB₁ neutral antagonist (AM6545), neither of which affected body weight when administered alone; (2) was absent in mice selectively lacking CB₁ in differentiated *AdipoQ*-expressing adipocytes^{37,38}; and (3) was not altered by a global CB₂ inverse agonist (AM630). The results reveal a previously unexpected contribution of CB₁ receptors to adipose organ homeostasis, which appears to be distinct from their known roles in energy conservation. In adult mammals, including humans, CB₁ activation stimulates food intake, heightens lipogenesis, and dampens non-shivering thermogenesis.^{6–8} We saw none of these effects in adolescent male mice, in which daily THC administration blunted the body-weight trajectory, reduced lean mass, increased EE, and decreased RER.

HFD. This state was accompanied by a striking molecular profile, characterized in both BAT and WAT by overexpression of proteins that are normally restricted to muscle and, in BAT only, by heightened anabolic processing. When given to young male adults, the same THC regimen did not significantly affect body weight gain and produced a more restricted set of transcriptional changes in the adipose organ, which did not include ectopic transcription of muscle genes. The results thus suggest that frequent exposure to low-dose THC during adolescence, but not adulthood, promotes an abnormal pseudo-lean state—a state that macroscopically resembles healthy leanness but is in fact associated with lasting impairments in the two hallmark functions of the adipose organ: thermogenesis and lipolysis.

These responses could not be ascribed to THC-induced adaptations in endocannabinoid signaling (e.g., CB₁ downregulation), which was minimally affected by THC treatment and disappeared in young adulthood. Their age dependence supports the possibility—suggested by prior work⁴³—that the function of the ECS may shift during adipose organ development from the regulation of adipocyte (trans)differentiation and adipogenesis in early life to the control of lipogenesis as animals mature.^{6–8}

Along with a pseudo-lean phenotype, adolescent THC exposure also caused pervasive transcriptional abnormalities in BAT and WAT. Many muscle-associated genes were induced in these tissues, whereas genes encoding for components of the mitochondrial respiratory chain were suppressed. Moreover,

Pgc1a levels were elevated in both BAT and WAT, while other critical regulators of adipocyte physiology were differentially affected—for example, *Adrb3* was down in BAT and up in WAT, while *Ucp1* was up in BAT and unchanged in WAT. Consistent with the transcriptional data, several sarcomere proteins—including titin, myosin, and troponin—were abnormally expressed in the BAT and WAT of THC-treated mice. One of them, titin, accumulated in brown adipocytes of THC-exposed animals, where it is not normally detectable. Interestingly, key proteins involved in mitochondrial respiration (e.g., NDUFA3 and 5, COX5A), whose transcription was suppressed, were increased in BAT after THC treatment. Mismatches between mRNA and protein levels are not uncommon⁴⁴ and are thought to reflect differences in temporal factors—such as protein half-life time and translation-rate constant—which might be exacerbated by the THC-mediated disruption of gene transcription and protein synthesis.

The anomalous molecular landscape induced by adolescent THC exposure defies straightforward interpretation. It is reasonable to speculate, however, that the adipose organ—independently or in cross-talk with other systems such as skeletal muscle^{45,46}—might adjust to inappropriate CB₁ activation during the second month of postnatal life, when the rate of adipocyte proliferation in rodents is particularly high,⁴⁷ by entering a lasting dyshomeostatic condition in which lipolysis is defective while thermogenesis and anabolic processing are enhanced. Whether a similar phenomenon occurs in adolescent humans, who also experience a rapid increase in adipose cell number and size during their teenage years,⁴⁸ is an important question for future studies.

The link between cannabis consumption, lower BMI, and improved cardiometabolic risk is well established in the epidemiological literature^{15–29} and cannot be ascribed to differences in lifestyle or to a tendency of lean individuals to become cannabis users.²⁰ In particular, longitudinal surveys have shown that continuous regular use of cannabis from adolescence (12–18 years) to adulthood (32–38 years) is associated with lower BMI, smaller waist-hip ratio, lower fasting triglyceride and glucose levels, and improved metabolic profile.^{14,15} To reconcile these findings with cannabis' propensity to stimulate palatable high-calorie eating,^{30–32} it has been proposed that habitual use of the drug might lead to a reduction in the number and/or signaling efficiency of CB₁ receptors. This hypothesis is inconsistent, however, with available evidence showing persistent hedonic eating³³ and increased carbohydrate and energy intake^{19,26} in people who regularly use cannabis in a non-medical setting. An intriguing alternative possibility suggested by our data is that the paradoxical metabolic profile of adult cannabis users might result, at least partly, from lasting modifications in adipose organ function induced by THC during adolescence. New data and resources emerging from the Adolescence Brain Cognitive Development (ABCD) and other long-term studies of child health may allow a test of this hypothesis.

In conclusion, the present results show that daily administration of low-dose THC in adolescent male mice results in an enduring metabolic state characterized by decreased fat mass, increased lean mass, partial resistance to diet-induced obesity and dyslipidemia, enhanced thermogenesis, and impaired stimulus-dependent lipolysis. Transcriptomic, proteomic, metabolo-

mic, and morphological analyses show that this state is accompanied by a complex set of molecular anomalies in BAT and WAT, which include overexpression of proteins that are normally found in skeletal and heart muscle. Whether such a state, which we refer to as pseudo-lean, might impact physical, social, and mental health is an important question for future investigations.

Limitations of study

Our experiments have several limitations, three of which are especially noteworthy. First, we found that adolescent THC treatment dampens body-weight gain in both male and female mice but focused our metabolic and molecular studies only on males. Since biological sex strongly influences energy homeostasis and adipose organ function,^{49,50} similar investigations should be conducted in female animals. Second, most of the molecular analyses presented here were carried out on BAT and WAT but, as suggested by the transcriptional changes observed in skeletal muscle, other organ systems may also be implicated in the response to THC. More generally, the body-wide impact of early-life exposure to THC remains understudied and the present findings underscore the need to fill this knowledge gap. Finally, our results do not shed light on the developmental context that renders differentiated adipocytes vulnerable to CB₁ receptor overactivation only during adolescence. Elucidating such context would advance our understanding of both the ECS and adipocyte plasticity.

STAR★METHODS

Detailed methods are provided in the online version of this paper and include the following:

- **KEY RESOURCES TABLE**
- **RESOURCE AVAILABILITY**
 - Lead contact
 - Materials availability
 - Data and code availability
- **EXPERIMENTAL MODEL AND SUBJECT DETAILS**
 - Animals
- **METHOD DETAILS**
 - Chemicals
 - Drug administration
 - Tissue collection
 - High-fat diet (HFD)-induced obesity
 - Body growth
 - Body composition
 - Feeding and motor activity
 - Energy expenditure
 - Blood chemistry
 - Efficiency of nutrient absorption
 - Glucose tolerance test
 - Temperature measurements
 - THC measurements
 - Endocannabinoid measurements
 - Morphological analyses
 - Quantitative real time reverse transcription PCR (RT-PCR)
 - Western blot analyses
 - Transcriptomic analyses

- Proteomic analyses
- Metabolomic analyses
- Gut microbiota tests
- **QUANTIFICATION AND STATISTICAL ANALYSIS**

SUPPLEMENTAL INFORMATION

Supplemental information can be found online at <https://doi.org/10.1016/j.cmet.2023.05.002>.

ACKNOWLEDGMENTS

This work was supported by the National Institute on Drug Abuse (P50DA044118-01 to D.P.). Additional funding was provided by grants R01DK121146 (to Q.Y.) and R01GM074830 and R35GM145249 (both to L.H.). The authors thank the researchers of the Genomics High-Throughput Facility (GHTF) and Microbiome Center in the University of California, Irvine, for assistance with microbiome analysis. The authors also thank Dr. Faizy Ahmed for assistance with LC-MS/MS analysis and Drs. Bruce Blumberg and Riann Egusquiza for discussion and access to MRI equipment.

AUTHOR CONTRIBUTIONS

D.P., L.L., and K.-M.J. designed the studies; L.L. performed the experiments with assistance from H.-L.L., F.P., E.S., S.S., A.T., and Y.F.; J.L. and C.J. carried out metabolomic analysis; C.Y. and L.H. performed proteomic analysis and G.C. and S.C. performed morphological analysis using electron microscope; C.W. and N.D. carried out experiments with conditional CB₁ knockout mice; L.T. and Q.Y. provided help with the metabolic chamber study; and D.P. ideated the project, supervised it, and wrote the manuscript with assistance from L.L., K.-M.J., C.J., and S.C.

DECLARATION OF INTERESTS

The authors declare no competing interests.

Received: July 27, 2022

Revised: February 7, 2023

Accepted: May 5, 2023

Published: June 1, 2023

REFERENCES

1. Lu, H.C., and Mackie, K. (2016). An introduction to the endogenous cannabinoid system. *Biol. Psychiatry* 79, 516–525. <https://doi.org/10.1016/j.biopsych.2015.07.028>.
2. Piomelli, D., and Mabou Tagne, A. (2022). Endocannabinoid-based therapies. *Annu. Rev. Pharmacol. Toxicol.* 62, 483–507. <https://doi.org/10.1146/annurev-pharmtox-052220-021800>.
3. Cinti, S. (2018). Adipose organ development and remodeling. *Compr. Physiol.* 8, 1357–1431. <https://doi.org/10.1002/cphy.c170042>.
4. DiPatrizio, N.V., and Piomelli, D. (2012). The thrifty lipids: endocannabinoids and the neural control of energy conservation. *Trends Neurosci.* 35, 403–411. <https://doi.org/10.1016/j.tins.2012.04.006>.
5. Piazza, P.V., Cota, D., and Marsicano, G. (2017). The CB1 receptor as the cornerstone of exostasis. *Neuron* 93, 1252–1274. <https://doi.org/10.1016/j.neuron.2017.02.002>.
6. Mazier, W., Saucisse, N., Gatta-Cherifi, B., and Cota, D. (2015). The endocannabinoid system: pivotal orchestrator of obesity and metabolic disease. *Trends Endocrinol. Metab.* 26, 524–537. <https://doi.org/10.1016/j.tem.2015.07.007>.
7. Ruiz de Azua, I., and Lutz, B. (2019). Multiple endocannabinoid-mediated mechanisms in the regulation of energy homeostasis in brain and peripheral tissues. *Cell. Mol. Life Sci.* 76, 1341–1363. <https://doi.org/10.1007/s00018-018-2994-6>.
8. Jung, K.M., Lin, L., and Piomelli, D. (2022). The endocannabinoid system in the adipose organ. *Rev. Endocr. Metab. Disord.* 23, 51–60. <https://doi.org/10.1007/s11154-020-09623-z>.
9. Quarta, C., and Cota, D. (2020). Anti-obesity therapy with peripheral CB1 blockers: from promise to safe(?) practice. *Int. J. Obes. (Lond)* 44, 2179–2193. <https://doi.org/10.1038/s41366-020-0577-8>.
10. Tam, J., Hinden, L., Drori, A., Udi, S., Azar, S., and Baraghithy, S. (2018). The therapeutic potential of targeting the peripheral endocannabinoid/CB(1) receptor system. *Eur. J. Intern. Med.* 49, 23–29. <https://doi.org/10.1016/j.ejim.2018.01.009>.
11. Mackie, K. (2008). Cannabinoid receptors: where they are and what they do. *J. Neuroendocrinol.* 20 (Suppl 1), 10–14. <https://doi.org/10.1111/j.1365-2826.2008.01671.x>.
12. Kreuz, D.S., and Axelrod, J. (1973). Delta-9-tetrahydrocannabinol: localization in body fat. *Science* 179, 391–393. <https://doi.org/10.1126/science.179.4071.391>.
13. Torrens, A., Vozella, V., Huff, H., McNeil, B., Ahmed, F., Ghidini, A., Mahler, S.V., Huestis, M.A., Das, A., and Piomelli, D. (2020). Comparative pharmacokinetics of Delta(9)-tetrahydrocannabinol in adolescent and adult male mice. *J. Pharmacol. Exp. Ther.* 374, 151–160. <https://doi.org/10.1124/jpet.120.265892>.
14. Meier, M.H., Caspi, A., Cerdá, M., Hancox, R.J., Harrington, H., Houts, R., Poulton, R., Ramrakha, S., Thomson, W.M., and Moffitt, T.E. (2016). Associations between cannabis use and physical health problems in early midlife: a longitudinal comparison of persistent cannabis vs tobacco users. *JAMA Psychiatry* 73, 731–740. <https://doi.org/10.1001/jamapsychiatry.2016.0637>.
15. Meier, M.H., Pardini, D., Beardslee, J., and Matthews, K.A. (2019). Associations between cannabis use and cardiometabolic risk factors: a longitudinal study of men. *Psychosom. Med.* 81, 281–288. <https://doi.org/10.1097/PSY.0000000000000665>.
16. Beulaygue, I.C., and French, M.T. (2016). Got munchies? Estimating the relationship between marijuana use and body mass index. *J. Ment. Health Policy Econ.* 19, 123–140.
17. Hayatbakhsh, M.R., O'Callaghan, M.J., Mamun, A.A., Williams, G.M., Clavarino, A., and Najman, J.M. (2010). Cannabis use and obesity and young adults. *Am. J. Drug Alcohol Abuse* 36, 350–356. <https://doi.org/10.3109/00952990.2010.500438>.
18. Barré, T., Pol, S., Ramier, C., Di Beo, V., Carrat, F., Bureau, M., Bourlière, M., Dorival, C., Serfaty, L., Asselah, T., et al. (2022). Cannabis use is inversely associated with overweight and obesity in hepatitis B virus-infected patients (ANRS CO22 Hepather cohort). *Cannabis Cannabinoid Res.* 7, 677–689. <https://doi.org/10.1089/can.2021.0094>.
19. Muniyappa, R., Sable, S., Ouwerkerk, R., Mari, A., Gharib, A.M., Walter, M., Courville, A., Hall, G., Chen, K.Y., Volkow, N.D., et al. (2013). Metabolic effects of chronic cannabis smoking. *Diabetes Care* 36, 2415–2422. <https://doi.org/10.2337/dc12-2303>.
20. Clark, T.M., Jones, J.M., Hall, A.G., Tabner, S.A., and Kmiec, R.L. (2018). Theoretical explanation for reduced body mass index and obesity rates in cannabis users. *Cannabis Cannabinoid Res.* 3, 259–271. <https://doi.org/10.1089/can.2018.0045>.
21. Alshaarawy, O., and Anthony, J.C. (2019). Are cannabis users less likely to gain weight? Results from a national 3-year prospective study. *Int. J. Epidemiol.* 48, 1695–1700. <https://doi.org/10.1093/ije/dyz044>.
22. Le Strat, Y., and Le Foll, B. (2011). Obesity and cannabis use: results from 2 representative national surveys. *Am. J. Epidemiol.* 174, 9–933. <https://doi.org/10.1093/aje/kwr200>.
23. Brook, J.S., Lee, J.Y., Finch, S.J., Balka, E.B., and Brook, D.W. (2013). Physical factors, personal characteristics, and substance use: associations with obesity. *Subst. Abuse.* 34, 273–276. <https://doi.org/10.1080/08897077.2013.770425>.
24. Danielsson, A.K., Lundin, A., Yaregal, A., Östenson, C.G., Allebeck, P., and Agardh, E.E. (2016). Cannabis use as risk or protection for type 2

- diabetes: a longitudinal study of 18 000 Swedish men and women. *J. Diabetes Res.* 2016. 6278709. <https://doi.org/10.1155/2016/6278709>.
25. Rajavashisth, T.B., Shaheen, M., Norris, K.C., Pan, D., Sinha, S.K., Ortega, J., and Friedman, T.C. (2012). Decreased prevalence of diabetes in marijuana users: cross-sectional data from the National Health and Nutrition Examination Survey (NHANES) III. *BMJ Open* 2. e000494. <https://doi.org/10.1136/bmjopen-2011-000494>.
26. Smit, E., and Crespo, C.J. (2001). Dietary intake and nutritional status of US adult marijuana users: results from the Third National Health and Nutrition Examination Survey. *Public Health Nutr.* 4, 781–786. <https://doi.org/10.1079/phn2000114>.
27. Penner, E.A., Buettner, H., and Mittleman, M.A. (2013). The impact of marijuana use on glucose, insulin, and insulin resistance among US adults. *Am. J. Med.* 126, 583–589. <https://doi.org/10.1016/j.amjmed.2013.03.002>.
28. Thompson, C.A., and Hay, J.W. (2015). Estimating the association between metabolic risk factors and marijuana use in U.S. adults using data from the continuous National Health and Nutrition Examination Survey. *Ann. Epidemiol.* 25, 486–491. <https://doi.org/10.1016/j.annepidem.2015.01.013>.
29. Warren, M., Frost-Pineda, K., and Gold, M. (2005). Body mass index and marijuana use. *J. Addict. Dis.* 24, 95–100. https://doi.org/10.1300/J069v24n03_08.
30. Greenberg, I., Kuehne, J., Mendelson, J.H., and Bernstein, J.G. (1976). Effects of marijuana use on body weight and caloric intake in humans. *Psychopharmacol. (Berl.)* 49, 79–84. <https://doi.org/10.1007/BF00427475>.
31. Foltin, R.W., Brady, J.V., and Fischman, M.W. (1986). Behavioral analysis of marijuana effects on food intake in humans. *Pharmacol. Biochem. Behav.* 25, 577–582. [https://doi.org/10.1016/0091-3057\(86\)90144-9](https://doi.org/10.1016/0091-3057(86)90144-9).
32. Haney, M., Gunderson, E.W., Rabkin, J., Hart, C.L., Vosburg, S.K., Comer, S.D., and Foltin, R.W. (2007). Dronabinol and marijuana in HIV-positive marijuana smokers. Caloric intake, mood, and sleep. *J. Acquir. Immune Defic. Syndr.* 45, 545–554. <https://doi.org/10.1097/QAI.0b013e31811ed205>.
33. Roberts, C.A., Jager, G., Christiansen, P., and Kirkham, T.C. (2019). Exploring the munchies: an online survey of users' experiences of cannabis effects on appetite and the development of a Cannabinoid Eating Experience Questionnaire. *J. Psychopharmacol.* 33, 1149–1159. <https://doi.org/10.1177/0269881119862526>.
34. Connor, J.P., Stjepanović, D., Le Foll, B., Hoch, E., Budney, A.J., and Hall, W.D. (2021). Cannabis use and cannabis use disorder. *Nat. Rev. Dis. Primers* 7, 16. <https://doi.org/10.1038/s41572-021-00247-4>.
35. Kelly, J.F., Bergman, B., Hoepfner, B.B., Vilsaint, C., and White, W.L. (2017). Prevalence and pathways of recovery from drug and alcohol problems in the United States population: implications for practice, research, and policy. *Drug Alcohol Depend.* 171, 162–169. <https://doi.org/10.1016/j.drugalcdep.2017.09.028>.
36. Lee, H.L., Jung, K.M., Fotio, Y., Squire, E., Palese, F., Lin, L., Torrens, A., Ahmed, F., Mabou Tagne, A., Ramirez, J., et al. (2022). Frequent low-dose delta(9)-tetrahydrocannabinol in adolescence disrupts microglia homeostasis and disables responses to microbial infection and social stress in young adulthood. *Biol. Psychiatry* 92, 845–860. <https://doi.org/10.1016/j.biopsych.2022.04.017>.
37. Hu, E., Liang, P., and Spiegelman, B.M. (1996). AdipoQ is a novel adipose-specific gene dysregulated in obesity. *J. Biol. Chem.* 271, 10697–10703. <https://doi.org/10.1074/jbc.271.18.10697>.
38. Emont, M.P., Jacobs, C., Essene, A.L., Pant, D., Tenen, D., Colleluori, G., Di Vincenzo, A., Jørgensen, A.M., Dashti, H., Stefek, A., et al. (2022). A single-cell atlas of human and mouse white adipose tissue. *Nature* 603, 926–933. <https://doi.org/10.1038/s41586-022-04518-2>.
39. Ruiz de Aza, I., Mancini, G., Srivastava, R.K., Rey, A.A., Cardinal, P., Tedesco, L., Zingaretti, C.M., Sassmann, A., Quarta, C., Schwitter, C., et al. (2017). Adipocyte cannabinoid receptor CB1 regulates energy homeostasis and alternatively activated macrophages. *J. Clin. Invest.* 127, 4148–4162. <https://doi.org/10.1172/JCI83626>.
40. Wong, A., Gunasekaran, N., Hancock, D.P., Denyer, G.S., Meng, L., Radford, J.L., McGregor, I.S., and Arnold, J.C. (2012). The major plant-derived cannabinoid Delta(9)-tetrahydrocannabinol promotes hypertrophy and macrophage infiltration in adipose tissue. *Horm. Metab. Res.* 44, 105–113. <https://doi.org/10.1055/s-0031-1297940>.
41. Szklarczyk, D., Gable, A.L., Nastou, K.C., Lyon, D., Kirsch, R., Pyysalo, S., Doncheva, N.T., Legeay, M., Fang, T., Bork, P., et al. (2021). The STRING database in 2021: customizable protein-protein networks, and functional characterization of user-uploaded gene/measurement sets. *Nucleic Acids Res.* 49, D605–D612. <https://doi.org/10.1093/nar/gkaa1074>.
42. Miech, R.A., Johnston, L.D., O'Malley, P.M., Bachman, J.G., Schulenberg, J.E., and Patrick, M.E. (2022). Monitoring the Future National Survey Results on Drug Use, 1975–2021: Volume I, Secondary School Students (Institute for Social Research, the University of Michigan). <http://monitoringthefuture.org/pubs.html#monographs>.
43. Bellocchio, L., Cervino, C., Vicennati, V., Pasquali, R., and Pagotto, U. (2008). Cannabinoid type 1 receptor: another arrow in the adipocytes' bow. *J. Neuroendocrinol.* 20 (Suppl 1), 130–138. <https://doi.org/10.1111/j.1365-2826.2008.01682.x>.
44. Buccitelli, C., and Selbach, M. (2020). mRNAs, proteins and the emerging principles of gene expression control. *Nat. Rev. Genet.* 21, 630–644. <https://doi.org/10.1038/s41576-020-0258-4>.
45. Shimizu, N., Maruyama, T., Yoshikawa, N., Matsumiya, R., Ma, Y., Ito, N., Tasaka, Y., Kuribara-Souta, A., Miyata, K., Oike, Y., et al. (2015). A muscle-liver-fat signalling axis is essential for central control of adaptive adipose remodelling. *Nat. Commun.* 6, 6693. <https://doi.org/10.1038/ncomms7693>.
46. Kong, X., Yao, T., Zhou, P., Kazak, L., Tenen, D., Lyubetskaya, A., Dawes, B.A., Tsai, L., Kahn, B.B., Spiegelman, B.M., et al. (2018). Brown adipose tissue controls skeletal muscle function via the secretion of myostatin. *Cell Metab.* 28, 631–643.e3. <https://doi.org/10.1016/j.cmet.2018.07.004>.
47. Greenwood, M.R., and Hirsch, J. (1974). Postnatal development of adipocyte cellularity in the normal rat. *J. Lipid Res.* 15, 474–483.
48. Knittle, J.L., Timmers, K., Ginsberg-Fellner, F., Brown, R.E., and Katz, D.P. (1979). The growth of adipose tissue in children and adolescents. Cross-sectional and longitudinal studies of adipose cell number and size. *J. Clin. Invest.* 63, 239–246. <https://doi.org/10.1172/JCI109295>.
49. Power, M.L., and Schulkin, J. (2008). Sex differences in fat storage, fat metabolism, and the health risks from obesity: possible evolutionary origins. *Br. J. Nutr.* 99, 931–940. <https://doi.org/10.1017/S0007114507853347>.
50. Shi, H., Seeley, R.J., and Clegg, D.J. (2009). Sexual differences in the control of energy homeostasis. *Front. Neuroendocrinol.* 30, 396–404. <https://doi.org/10.1016/j.yfrne.2009.03.004>.
51. Marsicano, G., Goodenough, S., Monory, K., Hermann, H., Eder, M., Cannich, A., Azad, S.C., Cascio, M.G., Gutiérrez, S.O., van der Stelt, M., et al. (2003). CB1 cannabinoid receptors and on-demand defense against excitotoxicity. *Science* 302, 84–88. <https://doi.org/10.1126/science.1088208>.
52. Sassmann, A., Offermanns, S., and Wettschureck, N. (2010). Tamoxifen-inducible Cre-mediated recombination in adipocytes. *Genesis* 48, 618–625. <https://doi.org/10.1002/dvg.20665>.
53. Chamorro-García, R., Shoucri, B.M., Willner, S., Käch, H., Janesick, A., and Blumberg, B. (2018). Effects of perinatal exposure to dibutyltin chloride on fat and glucose metabolism in mice, and molecular mechanisms, in vitro. *Environ. Health Perspect.* 126, 057006. <https://doi.org/10.1289/EHP3030>.
54. Gaetani, S., Oveisi, F., and Piomelli, D. (2003). Modulation of meal pattern in the rat by the anorexic lipid mediator oleoylethanolamide. *Neuropsychopharmacology* 28, 1311–1316. <https://doi.org/10.1038/sj.npp.1300166>.
55. Lin, L., Mabou Tagne, A., Squire, E.N., Lee, H.L., Fotio, Y., Ramirez, J., Zheng, M., Torrens, A., Ahmed, F., Ramos, R., et al. (2022). Diet-induced obesity disrupts histamine-dependent oleoylethanolamide signaling in the mouse liver. *Pharmacology* 107, 423–432. <https://doi.org/10.1159/000524753>.

56. Colleluori, G., Perugini, J., Di Vincenzo, A., Senzacqua, M., Giordano, A., and Cinti, S. (2022). Brown fat anatomy in humans and rodents. *Methods Mol. Biol.* 2448, 19–42. https://doi.org/10.1007/978-1-0716-2087-8_2.
57. Pfaffl, M.W., Tichopad, A., Prgomet, C., and Neuvians, T.P. (2004). Determination of stable housekeeping genes, differentially regulated target genes and sample integrity: BestKeeper–Excel-based tool using pair-wise correlations. *Biotechnol. Lett.* 26, 509–515. <https://doi.org/10.1023/b:bile.0000019559.84305.47>.
58. Schmittgen, T.D., and Livak, K.J. (2008). Analyzing real-time PCR data by the comparative C(T) method. *Nat. Protoc.* 3, 1101–1108. <https://doi.org/10.1038/nprot.2008.73>.
59. Palese, F., Pontis, S., Realini, N., and Piomelli, D. (2019). A protective role for N-acylphosphatidylethanolamine phospholipase D in 6-OHDA-induced neurodegeneration. *Sci. Rep.* 9, 15927. <https://doi.org/10.1038/s41598-019-51799-1>.
60. Wiśniewski, J.R., Zougman, A., Nagaraj, N., and Mann, M. (2009). Universal sample preparation method for proteome analysis. *Nat. Methods* 6, 359–362. <https://doi.org/10.1038/nmeth.1322>.
61. Guan, S., Price, J.C., Prusiner, S.B., Ghaemmaghami, S., and Burlingame, A.L. (2011). A data processing pipeline for mammalian proteome dynamics studies using stable isotope metabolic labeling. *Mol. Cell. Proteomics* 10, M111.010728. <https://doi.org/10.1074/mcp.M111.010728>.
62. Wollenberger, A., Ristau, O., and Schoffa, G. (1960). A simple technic for extremely rapid freezing of large pieces of tissue. *Pflugers Arch. Gesamte Physiol. Menschen Tiere* 270, 399–412.
63. Jung, S.M., Doxsey, W.G., Le, J., Haley, J.A., Mazuecos, L., Luciano, A.K., Li, H., Jang, C., and Guertin, D.A. (2021). In vivo isotope tracing reveals the versatility of glucose as a brown adipose tissue substrate. *Cell Rep.* 36, 109459. <https://doi.org/10.1016/j.celrep.2021.109459>.
64. Melamud, E., Vastag, L., and Rabinowitz, J.D. (2010). Metabolomic analysis and visualization engine for LC-MS data. *Anal. Chem.* 82, 9818–9826. <https://doi.org/10.1021/ac1021166>.
65. Bolyen, E., Rideout, J.R., Dillon, M.R., Bokulich, N.A., Abnet, C.C., Al-Ghalith, G.A., Alexander, H., Alm, E.J., Arumugam, M., Asnicar, F., et al. (2019). Reproducible, interactive, scalable and extensible microbiome data science using QIIME 2. *Nat. Biotechnol.* 37, 852–857. <https://doi.org/10.1038/s41587-019-0209-9>.
66. Bokulich, N.A., Dillon, M.R., Zhang, Y., Rideout, J.R., Bolyen, E., Li, H., Albert, P.S., and Caporaso, J.G. (2018). q2-longitudinal: longitudinal and paired-sample analyses of microbiome data. *mSystems* 3. <https://doi.org/10.1128/mSystems.00219-18>.
67. McDonald, D., Price, M.N., Goodrich, J., Nawrocki, E.P., DeSantis, T.Z., Probst, A., Andersen, G.L., Knight, R., and Hugenholtz, P. (2012). An improved Greengenes taxonomy with explicit ranks for ecological and evolutionary analyses of bacteria and archaea. *ISME J.* 6, 610–618. <https://doi.org/10.1038/ismej.2011.139>.

STAR★METHODS

KEY RESOURCES TABLE

REAGENT or RESOURCE	SOURCE	IDENTIFIER
Antibodies		
Anti-tyrosine hydroxylase antibody	Millipore Sigma	Millipore Cat# AB1542; RRID: AB_90755
Anti-CB ₁ receptor antibody	Abcam	Abcam Cat# ab181602; RRID: AB_2630358
Chemicals, peptides, and recombinant proteins		
AM6545	Cayman Chemicals	16316
AM251	Cayman Chemicals	71670
AM630	Cayman Chemicals	10006974
Δ9-THC (Tetrahydrocannabinol)	Cayman Chemicals	12068
Δ9-THC-D3 (Tetrahydrocannabinol-D3)	Cerilliant	T-011
OEA (oleoylethanolamide)	Cayman Chemicals	90265
PEA (palmitoylethanolamide)	Cayman Chemicals	10965
AEA (anadamide)	Cayman Chemicals	90050
2-AG (2-arachidonoylglycerol)	Cayman Chemicals	62160
Isoflurane	Pivotal veterinary	21295098
EDTA (0.5 M), pH 8.0	Thermo Fisher Scientific	AM9260G
Acetonitrile	Thermo Fisher Scientific	T001014000
Methanol	Thermo Fisher Scientific	T001024000
Water, HPLC grade	Thermo Fisher Scientific	WSSK-4
Formic acid	Thermo Fisher Scientific	A117-50
Invitrogen TRIzol	Thermo Fisher Scientific	15596026
Critical commercial assays		
Invitrogen PureLin RNA Mini Kit	Thermo Fisher Scientific	12-183-018A
Triglyceride Colorimetric Assay Kit	Cayman Chemicals	10010303
β-Hydroxybutyrate (Ketone Body) Colorimetric Assay Kit	Cayman Chemicals	700190
Deposited data		
Transcriptomic, proteomic, and metabolomic dataset	Deposited to DRYAD (datadryad.org)	https://doi.org/10.7280/D1KD8R
Experimental models: Organisms/strains		
Mouse: C57BL/6J	Jackson Laboratories	Strain #:000664; RRID: IMSR_JAX:000664
Mouse: CB1f/f	Marsicano et al. ⁵¹	N/A
Mouse: AdipoqCreERT2tg/+	Sassmann et al. ⁵²	N/A
Oligonucleotides		
TaqMan Assay, <i>Actb</i>	Thermo Fisher Scientific	Mm00607939_s1
TaqMan Assay, <i>Adrb3</i>	Thermo Fisher Scientific	Mm00442669_m1
TaqMan Assay, <i>Cnr1</i>	Thermo Fisher Scientific	Mm01212171_s1
TaqMan Assay, <i>Dagla</i>	Thermo Fisher Scientific	Mm00813830_m1
TaqMan Assay, <i>Faah</i>	Thermo Fisher Scientific	Mm00515684_m1
TaqMan Assay, <i>Gapdh</i>	Thermo Fisher Scientific	Mm99999915_g1
TaqMan Assay, <i>Hprt</i>	Thermo Fisher Scientific	Mm00446968_m1
TaqMan Assay, <i>Mgl1</i>	Thermo Fisher Scientific	Mm00449274_m1
TaqMan Assay, <i>Napepld</i>	Thermo Fisher Scientific	Mm00724596_m1
TaqMan Assay, <i>Ppargc1a</i>	Thermo Fisher Scientific	Mm00447179_m1
See Table S2 for <i>Pparg</i> , <i>Prdm16</i> , <i>Ucp1</i> , <i>Ucp2</i> , <i>Ucp3</i>	N/A	N/A

(Continued on next page)

Continued

REAGENT or RESOURCE	SOURCE	IDENTIFIER
Software and algorithms		
ImageJ	(https://imagej.nih.gov/ij/download.html)	N/A
GraphPad Prism	GraphPad Prism	version 8.0
MassHunter	Agilent Technologies	N/A
STRING	(https://string-db.org)	N/A
Other		
high-fat diet (60% kcal fat)	Research Diets	D12492

RESOURCE AVAILABILITY

Lead contact

Further information and requests for resources and reagents should be directed to and will be fulfilled by the Lead Contact, Dr. Daniele Piomelli (piomelli@hs.uci.edu).

Materials availability

This study did not generate new unique reagents.

Data and code availability

- Transcriptomic, proteomic, and metabolomic data have been deposited in DRYAD and are publicly available as of the date of publication. Accession numbers are listed in the [key resources table](#). [Data S1](#) refers to unprocessed data underlying the display items in the manuscript, related to all main and supplemental figures.
- This paper does not report original code.
- Any additional information required to reanalyze the data reported in this paper is available from the lead contact upon request.

EXPERIMENTAL MODEL AND SUBJECT DETAILS

Animals

We obtained C57BL/6J mice of both sexes from Jackson Laboratories (Farmington, CT). Conditional adipose tissue-CB₁-knockout (Ati-CB₁-KO) mice were generated by crossing AdipoqCreERT2 mice⁵² with mice containing two loxP sites flanking the open reading frame of the *Cnr1* gene.^{39,51} Tamoxifen treatment began at PND14 and consisted of 5 daily intraperitoneal (IP) injections of 40 mg/kg in 4 mL of corn oil. Mice were transferred back to their home cages 72 h after the final tamoxifen injection. All animals were housed in ventilated cages (4–5 per cage) with food and water available ad libitum. Age- and weight-matched animals were randomly assigned to treatment groups and were allowed to acclimate for at least one week before experiments. Housing rooms were maintained on a 12-h light/12-h dark cycle (lights on at 6:30 AM) with constant temperature (20±2°C) and relative humidity (55–60%). All procedures were approved by the Institutional Animal Care and Use Committee of the University of California Irvine, and were carried out in strict accordance with the National Institutes of Health guidelines for the care and use of experimental animals.

METHOD DETAILS

Chemicals

We purchased AM251, AM6545, AM630, oleoylethanolamide (OEA), palmitoylethanolamide (PEA), anandamide (AEA), 2-arachidonoyl-*sn*-glycerol (2-AG), and THC from Cayman Chemicals (Ann Arbor, MI). CL316,243 was from Tocris Biosciences (Bristol, UK) and [²H₃]-THC was from Cerilliant (Round Rock, TX). Other deuterium-containing standards were from Cayman Chemicals. Liquid chromatography (LC) solvents and all other chemicals were from Sigma Aldrich (Saint Louis, MO) or Honeywell (Muskegon, MI, USA). Formic acid was from Thermo Fisher Scientific (Waltham, MA). All solvents and chemicals were of the highest available grade.

Drug administration

Drugs were freshly prepared and administered by IP injection. THC was dissolved in a vehicle of Tween 80/sterile saline (5:95, v/v) and was administered once daily on PND30–43, unless specified otherwise. We selected a dose of THC (5 mg/kg) that, in male mice, is known to produce (i) peak plasma concentrations of the drug that are comparable to those measured in humans after smoking a single cannabis cigarette (containing 3.4% THC); and (ii) modest pharmacological effects, including a submaximal decrease in body temperature and no change in motor activity or food intake.^{13,36} AM251, AM6545 and AM630 were dissolved in dimethyl sulfoxide (DMSO) in sterile saline (5:95, v/v) and administered by IP injection 60 min before THC.

Tissue collection

Mice were anesthetized with isoflurane (Pivotal veterinary, Loveland, CO), and cardiac blood was collected into ethylenediaminetetraacetic acid (EDTA)-rinsed syringes and transferred into 1 ml polypropylene plastic tubes containing spray-coated potassium-EDTA. Blood was centrifuged at $1,450 \times g$ at 4°C for 15 min and supernatants were transferred into polypropylene tubes. The animals were decapitated and interscapular BAT, epididymal WAT, and hindlimb quadriceps muscle were quickly removed, snap-frozen and stored at -80°C until analyses.

High-fat diet (HFD)-induced obesity

Groups of C57BL/6 mice received either vehicle (Tween 80/sterile saline, 5:95, v/v) or THC (5 mg/kg, IP) on PND30–43. Starting from PND57, they were exposed to a high-fat diet (HFD, 60 kcal % fat, D12492; Research Diets, New Brunswick, NJ) for 10 weeks. Body weight and food intake were recorded three times per week.

Body growth

Mice were lightly anesthetized with isoflurane and body, tail and head length were measured using a ruler, holding the animals by the tail.

Body composition

Body composition was measured on PND44, PND70 and PND130 (HFD-exposed group), using an EchoMRI Whole Body Composition Analyzer (EchoMRI, Houston, TX) as described.⁵³

Feeding and motor activity

Feeding and motor activity were recorded using an automated system (SciPro, New York, NY), as described.⁵⁴ Mice were habituated to test cages for 5 days prior to trials. 24-h food intake (g/weight) and motor activity were measured. We assessed the following feeding parameters: average satiety ratio [min/(g/kg)], feeding latency (min), meal size (g/kg), post meal interval (min), meal frequency (meals/h) and duration.⁵⁴

Energy expenditure

Mice were individually acclimated to metabolic chambers (PhenoMaster System, TSE, Germany) for 24 h. Motor activity, O_2 consumption, and CO_2 production were recorded at 30-min intervals for 3 consecutive days. Body weight and food intake were measured before and after the tests.

Blood chemistry

Plasma samples (0.1 ml) were prepared from cardiac blood obtained from mice at PND44, PND70, and PND130 (HFD-exposed group) after overnight fasting. Analyses were conducted at Antech Diagnostics (Irvine, CA). Free fatty acids were measured using a colorimetric assay kit (Abcam, Cambridge, UK).

Efficiency of nutrient absorption

Fecal matter (~ 0.5 g) was collected on PND43–44 and PND69–70 from group-housed mice (4 per cage). The samples were frozen in liquid N_2 , pulverized in a mortar, and transferred to 16-ml glass tubes. Sterile saline (5 ml) and chloroform/methanol (2:1, v/v; 5 ml) were added, the samples were stirred vigorously and centrifuged at $1,000 \times g$ for 15 min at 4°C . The organic phases were collected and dried under N_2 . Extracts were reconstituted in NP40 substitute assay reagent (Cayman Chemical) containing protease inhibitors. Triglycerides were quantified using a colorimetric assay kit (Cayman Chemical).

Glucose tolerance test

On PND130, HFD-exposed mice were food deprived overnight in cages equipped with a wired bottom (to prevent coprophagia). Three h prior to the test, the animals were placed in new cages in a quiet room. During the test, body weight was recorded, and 20% glucose (1 g of glucose/kg body weight) was administered by IP injection. Tail blood was collected before and 15, 30, 60 and 120 min after injections. Glucose concentrations were measured using a commercial instrument (Aviva, ACCU-CHEK, Indianapolis, IN).

Temperature measurements

Under light isoflurane anesthesia, we implanted and fixed with surgical glue temperature microchips (United Information Devices, Lake Villa, IL) in the mouse peritoneum at PND68. Animals were returned to their home cages for 24 h. On PND69, we recorded baseline temperature during the light and dark phases. On PND70, the animals were transferred to a walk-in cold room (4°C) and temperature was measured at periodic intervals for the following 6.5 h.

THC measurements

THC extraction

Epididymal adipose tissue (15–20 mg) was transferred into 2-ml Precellys tubes (Bertin Instruments, France) and homogenized in ice-cold acetonitrile (0.5 ml) containing 1% formic acid and [$^2\text{H}_3$]-THC (50 pmol) as internal standard. The samples were stirred vigorously

for 30 s and centrifuged at 2,800 x g at 4°C for 15 min. Supernatants were loaded onto Captiva Enhanced Matrix Removal (EMR) cartridges (Agilent Technologies, Santa Clara, CA) prewashed with water/acetonitrile (1:4, v/v). The extracts were eluted under positive pressure (3–5 mmHg, 1 drop/5 sec) using a Positive Pressure manifold 48 processor (PPM-48, Agilent Technologies). Tissue pellets were rinsed with water/acetonitrile (1:4, v/v; 0.2 ml), stirred for 30 s, and centrifuged again at 2,800 x g at 4°C for 15 min. The supernatants were transferred onto EMR cartridges, eluted, and pooled with the first eluate. The cartridges were washed again with water/acetonitrile (1:4, v/v; 0.2 ml), and pressure was increased gradually to 10 mmHg (1 drop/sec) to ensure maximal analyte recovery. Eluates were dried under N₂ and reconstituted in methanol (0.1 ml) containing 0.1% formic acid and transferred to deactivated glass inserts (0.2 ml) placed inside amber glass vials (2 ml; Agilent Technologies).

LC/MS-MS analysis

LC separations were carried out using a 1200 series LC system coupled with a 6410B mass spectrometric detector (Agilent Technologies). Analytes were separated on an Eclipse XDB C18 column, 1.8- μ m, 2.1 x 50 mm (Agilent Technologies). The mobile phase consisted of water containing 0.1% formic acid as solvent A and methanol containing 0.1% formic acid as solvent B. The flow rate was 0.5 ml/min. The gradient conditions were as follows: starting 75% B to 89% B in 3.0 min, changed to 95% B at 3.01 min and maintained till 4.5 min to remove any strongly retained materials from the column followed by column re-equilibration with 75 % B for 2.5 min. The total analysis time, including re-equilibrium, was 7 min. The column temperature was maintained at 40°C and the autosampler at 9°C. The injection volume was 2.0 μ l. To prevent carry-over, the needle was washed in the autosampler port for 30 s before each injection using a wash solution consisting of 10% acetone in water/methanol/isopropanol/acetonitrile (1:1:1:1, v/v). The mass spectrometer was operated in the positive electrospray ionization mode, and THC/internal standard were quantified by multiple reaction monitoring (MRM) using transitions listed in table below. Capillary voltage was set at 3,500 V. Source temperature was 300°C, and gas flow was set at 12.0 l/min. Nebulizer pressure was set at 40 psi. Collision energy and fragmentation voltage were set as reported.¹³ The MassHunter software (Agilent Technologies) was used for instrument control, data acquisition, and data analysis.

Acquisition parameters for Δ^9 -tetrahydrocannabinol (THC), anandamide (AEA), oleoylethanolamide (OEA), palmitoylethanolamide (PEA), 2-AG and their deuterium-containing analogs used as internal standards (ISTD)

Compound	Precursor (m/z)	Product (m/z)	Dwell time (ms)	Fragmentation (V)	Collision (V)	ESI Polarity
THC	315.25	193.1	200	145	21	+ve
[² H ₃]-THC (ISTD)	318.25	196.1	200	145	21	+ve
OEA	326.33	62.2	200	116	14	+ve
[² H ₄]-OEA (ISTD)	330.33	66.2	200	116	14	+ve
PEA	300.29	62.2	200	132	14	+ve
[² H ₄]-PEA (ISTD)	304.32	66.2	200	127	14	+ve
AEA	348.29	62.2	200	132	14	+ve
[² H ₄]-AEA (ISTD)	352.32	66.2	200	127	14	+ve
2-AG	379.29	287.2	200	142	10	+ve
[² H ₅]-2-AG (ISTD)	384.33	287.2	200	142	10	+ve

Endocannabinoid measurements

Tissue extraction

Frozen epididymal WAT and interscapular BAT samples (~40 mg) were transferred to 2 ml Precellys soft tissue vials (Bertin Instruments) and ice-cold acetone (1 ml) containing [²H₄]-anandamide and [²H₅]-2-AG (100 nmol each) was added. The samples were homogenized at 4°C at 6,800 rpm, 15 s per cycle for two cycles with a 20-s pause. They were then centrifuged at 830 x g for 15 min at 4°C and supernatants were eluted over EMR-Lipid cartridges, as described above. Eluates were dried under N₂, reconstituted in acetonitrile (0.1 ml), and stored at -20°C until analysis.

LC/MS-MS analysis

Endocannabinoids were fractionated using a 1260 series LC system (Agilent Technologies) coupled to a 6460C triple-quadrupole mass spectrometric detector (MSD; Agilent), as described.⁵⁵ A step gradient separation was performed on a Poroshell 120 column 1.9 μ m, 2.1 x 100 mm (Agilent Technologies) with a mobile phase consisting of 0.1% formic acid in water as solvent A and 0.1% formic acid in acetonitrile as solvent B. A linear gradient was used: 0.0–9.5 min 55.0 % B - 80% B; 9.51–11.0 min 95% B; and 11.01–15.50 min maintained at 55% B for column re-equilibration. Column temperature was 40°C and autosampler temperature at 9°C. Injection volume was 2 μ l, flow rate was 0.3 ml/min, and total analysis time, including column re-equilibration, was 15.5 min. To prevent carry-over, the needle was washed in the autosampler port for 30 s before each injection using a wash solution consisting of 10% acetone in water/methanol/isopropanol/acetonitrile (1:1:1:1, v/v). The mass spectrometer was operated in the positive electrospray ionization mode, and analytes were quantified using the MRM transitions listed in Methods Table M1. Capillary and nozzle voltages were set at 3,500 V and 500V respectively. Drying gas and sheath temperatures were 300°C with gas flows of 9.0 L/min and 12 L/min. Nebulizer pressure was set at 40 psi. MassHunter software (Agilent Technologies) was used for instrument control, data acquisition, and data analysis.

Morphological analyses

Measurement of adipocyte area

Epididymal WAT was fixed by overnight incubation in phosphate-buffered saline (PBS, 0.1 M, pH 7.4) containing 4% paraformaldehyde (PFA). The samples were rinsed, dehydrated, cleared, and embedded in paraffin. Sections (7 μ m thickness) were prepared using a Leica microtome RM2255 (Leica Biosystems, Deer Park, IL). Sections were dehydrated in ethanol, cleared, mounted, and stained with hematoxylin/eosin (National Diagnostics, Atlanta, GA). Transilluminated images of H&E-stained tissues were collected using a Ti Eclipse Microscope (Nikon, Melville, NY) with a Plan Apo 10 x objective. Images were analyzed using the NIH image J software.

Immunohistochemistry

Samples were processed as described.⁵⁶ Briefly, mice were anesthetized and perfused with PBS through the heart, followed by 4% PFA in 0.1M PBS at pH 7.4. Interscapular BAT and epididymal WAT were dissected and fixed overnight at 4°C. The samples were stored in 0.1% PFA at 4°C until processing. Fixed samples were dehydrated and embedded in paraffin. De-waxed sections were stained with either an anti-tyrosine hydroxylase antibody (Cat#AB1542, Millipore Sigma, Burlington, MA) or an anti-titin antibody (Polyclonal Rabbit PA5-68473, Thermo Fisher Scientific) which were detected using the ABC method (Vector Laboratories, Newark, CA). Morphometric analyses were performed to assess the size of the lipid droplets. For this purpose, tissue sections were observed using a Nikon Eclipse E800 light microscope and digital images were acquired at 40X magnification with a Nikon DXM 1220 camera. For each sample, 5 tissue sections, at least 500 μ m apart from each other, were selected. The size of at least 2,500 lipid droplets was measured for each sample (5 different areas per sample, 4 samples per condition). Data were analyzed using ImageJ.

Electron microscopy

Small pieces of WAT and BAT tissue (2-3 mm³) were fixed in 2% glutaraldehyde, 2% paraformaldehyde in 0.1 M phosphate buffer, pH 7.4, overnight at room temperature. Samples were post-fixed in 2% OsO₄ and 2% K-Ferrocyanide (1:1) for 60 min at 4°C and dehydrated with increasing concentration of acetone (60% and 100% in H₂O for 25 min each at room temperature). Samples were incubated with a mixture of epoxy-resin/acetone (1:1 and 2:1) and then with absolute epoxy-resin for 20 min at 60°C. Embedding in epoxy resin was performed using a silicon rubber mold (overnight at 60°C). Semithin sections (1500 nm) were made using a microtome to identify the region of interest to be studied. Lastly, ultrathin sections (64 nm) of the region of interest were prepared with an MTX ultramicrotome (RMC, Tucson, AZ), placed on a 1 mm-diameter grid (300 mesh nickel), stained with lead citrate, and imaged using a Philips CM10 transmission electron microscope (Philips, Eindhoven, Netherlands) as previously described.⁵⁶

Quantitative real time reverse transcription PCR (RT-PCR)

First-strand cDNA was amplified using the TaqMan Universal PCR Master Mix, following manufacturer's instructions. Primers and fluorogenic probes were purchased from Applied Biosystems (TaqMan(R) Gene Expression Assays, Foster City, CA) (see table below) and performed in 96-well plates using a CFX96 Real-Time System (Bio-Rad, Hercules, CA). Thermal cycling conditions were as follows: initial denaturation step at 95°C for 10 min, followed by 45 cycles, where each cycle was performed at 95°C for 30 s followed by 65°C for 60 s. Comparative quantitation of gene expression was conducted using the 2- $\Delta\Delta$ Ct method, with vehicle control as the calibrator. Expression of target genes was normalized using the Best-keeper software⁵⁷ using *Actb*, *Hprt*, and *Gapdh*.⁵⁸ Data are reported as fold change relative to control groups.

Gene Target	Assay ID (Thermo Fisher Scientific Taqman Assays)
<i>Actb</i>	Mm00607939_s1
<i>Adrb3</i>	Mm00442669_m1
<i>Cnr1</i>	Mm01212171_s1
<i>Dagla</i>	Mm00813830_m1
<i>Faah</i>	Mm00515684_m1
<i>Gapdh</i>	Mm99999915_g1
<i>Hprt</i>	Mm00446968_m1
<i>Mgll</i>	Mm00449274_m1
<i>Napepld</i>	Mm00724596_m1
<i>Pgc1a (Ppargc1a)</i>	Mm00447179_m1
<i>Pparg</i>	Mm00440940_m1
<i>Prdm16</i>	Mm00712556_m1
<i>Ucp1</i>	Mm01244861_m1
<i>Ucp2</i>	Mm00627599_m1
<i>Ucp3</i>	Mm00494077_m1

Western blot analyses

These were performed as described⁵⁹ with minor modifications. Briefly, proteins (30 μ g) were denatured in SDS (8%) and β -mercaptoethanol (5%) at 95 °C for 5 min. After separation by SDS-PAGE on a 4–15% gel, the proteins were electrotransferred to nitrocellulose membranes. The membranes were blocked with 0.2% Tropix I-Block (Thermo Fisher Scientific) in PBS, pH 7.4, containing 0.1% Tween-20 at room temperature for 1 h. They were then incubated overnight at 4 °C with either an anti-CB₁ receptor rabbit monoclonal antibody (D5N5C, #93815, Cell Signaling Technology, Danvers, MA) or an anti-GAPDH rabbit monoclonal antibody (#ab181602, Abcam, Cambridge, UK) at 1:1,000 dilution in 0.2% Tropix I-Block in PBS, pH 7.4, containing 0.1% Tween-20, as the loading control. This was followed by incubation with a secondary horseradish peroxidase-linked antibody (1:5,000, Millipore Sigma) in Tris-buffered saline (TBS), pH 7.4, containing 0.1% Tween-20 at room temperature for 1 h. Finally, proteins were visualized using an ECL kit (Bio-Rad, USA) and the chemiluminescence image was recorded using a LAS-4000 lumino-image analyzer system (Fujifilm, Tokyo, Japan).

Transcriptomic analyses

RNA isolation

Total RNA was extracted as described.³⁶ Samples with RNA integrity number ≥ 8.5 were used for RNA sequencing.

RNA sequencing and bioinformatics analyses

RNA sequencing was conducted at Novogene (Beijing, People's Republic of China) using the Illumina NovaSeq platform with paired-end 150 bp (PE 150) sequencing strategy. Downstream bioinformatic analyses were performed using a combination of programs including STAR, HTseq, Cufflink and Novogene's wrapped scripts, and alignments were parsed using STAR. Principal component analysis and comparative analyses of differentially expressed genes (DEGs) between test groups were performed using the DESeq2/edgeR package and a model based on negative binomial distribution. Resulting P values were adjusted using the Benjamini and Hochberg's approach for controlling false discovery rate (Adjusted P values, Padj). For transcriptome analysis, comparative analysis of DEGs was carried out between two test groups. Changes displaying Padj < 0.05 were considered significant. DEG distribution was assessed using Volcano plots showing statistical significance (Padj) vs magnitude of change (fold change). DEGs were annotated using the Database for Annotation, Visualization and Integrated Discovery (DAVID) database, PANTHER gene ontology (GO) knowledgebase, and the Kyoto Encyclopedia of Genes and Genomes (KEGG) pathway database, which was implemented using the ClusterProfiler and/or iDep.93 bioinformatics platform. GO terms with adjusted P value less than 0.05 were considered significantly enriched in DEGs.

Proteomic analyses

Tissue processing

WAT and BAT samples (~50 mg) were transferred in ice-cold 2.0 ml Precellys soft tissue tubes in radioimmunoprecipitation lysis buffer (Cell Signaling Technology, Boston, MA) containing a protease inhibitor cocktail (Halt Protease, Thermo Fisher Scientific; 1/100 dilution) and a phosphatase inhibitor cocktail (Sigma Aldrich; 1/100 dilution). Samples were homogenized using a Bertin homogenizer at 4 °C, 15 s/cycle for 2 cycles with 20 s pause between cycles and 45-s sample chilling time. The homogenates were transferred into 1.5 ml tubes, centrifuged for 15 min at 6,000 $\times g$ and 4 °C, and the liquid collected under the fat layer was carefully transferred into another 1.5 ml tube using a 25G needle. The procedure was repeated twice. Protein concentration was measured using the bicinchoninic acid (BCA) method (Thermo Fisher Scientific), following manufacturer's instructions.

Sample preparation for LC-MS/MS

The lysates were digested using a modified filter-assisted sample preparation protocol⁶⁰ over 10 kDa Microcon centrifugal filters (Millipore Sigma). Samples were reduced on-filter using 4 mM TCEP (tris(2-carboxyethyl) phosphine) (Thermo Fisher Scientific) at room temperature for 30 min, followed by alkylation using 8 mM iodoacetamide (Sigma Aldrich) at room temperature for 30 min. The proteins were digested for 4 h at 37 °C in 8 M urea using Lys-C (Wako Chemicals, Richmond, VA), followed by overnight trypsin digestion at 37 °C after diluting the concentration of urea to < 1.5 M. Peptide mixtures were cleaned using a Waters Sep-Pak tC18 cartridge, vacuum centrifuged, and resuspended in 3% acetonitrile/2% formic acid sample buffer prior to MS analysis. Peptide mixtures were subjected to LC-MS/MS analysis using an UltiMate 3000 RSLC (Thermo Fisher Scientific) coupled to an Orbitrap Fusion Lumos mass spectrometer (Thermo Fisher Scientific).

LC-MS/MS: LC separation was performed on a 50 cm \times 75 μ m I.D. Acclaim PepMap RSLC column. Peptides were eluted using a gradient of 3% to 22% acetonitrile in water containing 0.1% formic acid at a flow rate of 300 nL/min over 90 min. MS/MS spectra were extracted from RAW spectrometric files using PAVA⁶¹ and were searched using Batch-Tag within Protein Prospector (v.6.3.5) against a decoy-containing database consisting of a normal *Mus musculus* Swissprot database concatenated with a randomized version (SwissProt.2019.4.8.random.concat, total of 17,016 protein entries). The mass accuracy for parent ions and fragment ions were set as ± 20 ppm and 0.6 Da, respectively. Trypsin was set as the enzyme, and a maximum of two missed cleavages were allowed. Protein N-terminal acetylation, methionine oxidation, and N-terminal conversion of glutamine to pyroglutamic acid were selected as variable modifications. The false detection rate for proteins and peptides was set at 1%. For each analysis, the number of unique peptides, total number of peptides, and protein coverage were determined. Quantitation of the proteins was performed in MaxQuant using similar settings as Protein Prospector searches. Briefly, RAW files were searched using MaxQuant (v. 1.6.0.16) against a FASTA containing the *Mus musculus* proteome obtained from the SwissProt open-source database (version December 2020). The first search peptide tolerance was set to 20 ppm, with main search peptide tolerance set to 4.5 ppm. The protein, peptide,

and peptide spectrum match level false discovery rates were all 1%, as determined by a target-decoy approach. For quantification, intensities were determined as the full peak volume over the retention time profile. The degree of uniqueness required for peptides to be included in quantification was “Unique plus razor peptides.” The resulting label-free quantification (LFQ) values calculated using MaxQuant were used for comparing protein relative abundance among different samples.

Metabolomic analyses

Interscapular BAT and epididymal WAT were harvested and snap frozen in liquid N₂ using a pre-cooled Wollenberger clamp.⁶² Samples (~50 mg) were pulverized to a homogeneous powder using a Cryomill (Retsch, Newtown, PA). An ice-cold mixture of methanol:acetonitrile:water (40:40:20, v/v; 0.5–0.6 mL) was added to ~10–15 mg of powdered samples to make 25 mg/ml suspensions, which were centrifuged at 16,000 × *g* for 10 min at 4°C. Supernatants (3 μL) were analyzed as described.⁶³ Briefly, a quadrupole-orbitrap mass spectrometer (Q Exactive Plus, Thermo Fisher Scientific) operated in negative ionization mode was coupled to a Vanquish Ultra High-Performance LC system (Thermo Fisher Scientific) with electrospray ionization. Scan range was *m/z* 70–1000, scanning frequency was 1 Hz and resolution was 140,000. LC separations were conducted using a XBridge BEH Amide column (2.1 mm × 150 mm, 2.5 mm particle size, 130Å pore size) with a gradient consisting of solvent A (20 mM ammonium acetate, 20 mM ammonium hydroxide in 95:5 water:acetonitrile, pH 9.45) and solvent B (acetonitrile). Flow rate was 150 μL/min. The gradient was: 0 min, 85% B; 2 min, 85% B; 3 min, 80% B; 5 min, 80% B; 6 min, 75% B; 7 min, 75% B; 8 min, 70% B; 9 min, 70% B; 10 min, 50% B; 12 min, 50% B; 13 min, 25% B; 16 min, 25% B; 18 min, 0% B; 23 min, 0% B; 24 min, 85% B; 30 min, 85% B. Autosampler temperature was 4°C. Data were analyzed using the MAVEN software.⁶⁴ To control for instrument variability, an internal standard, [¹⁵N]-valine, was spiked in the extraction solvent.

Gut microbiota tests

Fecal sample preparation

Mixed fecal droppings (~2 ml in volume) were collected from 4 mice in each cage at PND 44 (n=3 cages per group) and PND 70 (n=4 cages per group). Fecal samples were placed into 15 ml tubes and immediately stored in the -80 °C freezer. Samples were kept at -80°C and thawed once to extract the DNA for 16S rRNA sequencing.

Preparation of DNA and 16S library construction for Illumina sequencing

Extraction of DNA from frozen stool samples was performed using the Qiamp DNA stool mini kit according to manufacturer's instructions. Approximately 180–200 mg of stool sample was used for the DNA extraction. The resulting DNA was measured by Qubit and 5 ng was used as input for library construction. The library preparation was performed according to the Illumina 16S Metagenomic Sequencing Library Preparation protocol. More specifically, the protocol includes the primer pair sequences for the V3 and V4 region that create a single amplicon of approximately ~460 bp [16S Amplicon Forward (V3 region): 5'-TCGTCGGCAGCGTCAGATGTGATAAGAGACAGCCTACG GNGGCCWGCAG-3, and 16S Amplicon Reverse (V4 region): 5'-GTCTCGTGGGCTCGGAGATGTGTATAAGAGACAGGACTACHVGGGTATCTAATCC-3'].

The protocol also includes overhang adapter sequences that must be appended to the primer pair sequences for compatibility with Illumina index and sequencing adapters. Primers for the second step PCR reaction were used from the dual index kit for Nextera XT library construction. The resulting libraries were assayed for quantity using Qubit and for quality using the Agilent Bioanalyzer 2100 DNA HS chip. The libraries were normalized and then multiplexed together. The multiplexed library pool was quantified using qPCR and sequenced on Illumina Miseq 2X300bp run.

Analysis

We imported 3.4 million demultiplexed Illumina Miseq sequence reads into QIIME2 version 2018.11⁶⁵ (<https://qiime2.org>). After quality control, we continued the analysis with the forward read only. We used DADA2 to denoise the single end forward reads with operational taxonomical units (OTUs), OTUs picked at 100% similarity. We assigned taxonomy to the OTUs with representatives' sequences and the classifier trained with the q2-feature-classifier, classify-sklearn naïve Bayes taxonomy classifier against the greengenes database 13.8 99% OTUs reference sequences.^{66,67} The QIIME2 created OTU table as well as the taxonomy table and metadata were transferred into R for statistical analysis (R version 4.0.2). We rarefied the OTU table via randomized sampling without replacement with 100 iterations at 124139 sequences per sample using the “EcolUtils” package (R core Team, 2018, <https://www.r-project.org/>; Salazar, G. 2020. EcolUtils: Utilities for community ecology analysis. <https://github.com/GuillemSalazar/EcolUtils>). We determined the effect of age and treatment and its interaction on microbial composition with Permutational multivariate analysis of variance (PERMANOVA) on a Bray Curtis dissimilarity matrix that was generated from the rarefied OTU table using the *adonis* function of the *vegan* package version 2.5-6 in R. We performed a Shapiro-Wilk test to check for normality distribution of residuals for the Shannon diversity. Since the distribution was normal an ANOVA was used to check for significance of any of the factors for alpha diversity.

QUANTIFICATION AND STATISTICAL ANALYSIS

Results are expressed as means ± SEM. Significance was determined using unpaired, two-tailed Student's *t* test or analysis of variance (ANOVA) (one way, two way) followed by Tukey's or Bonferroni's post hoc tests, as appropriate. GraphPad Prism version 8.0 (GraphPad Prism, San Diego, CA) was used to perform the analysis. Differences were considered significant if *P* < 0.05. Analysis of transcriptomics, metabolomics and proteomics results were conducted as described in previous sections.